EUROPEAN RESPIRATORY journal

FLAGSHIP SCIENTIFIC JOURNAL OF ERS

Early View

Original article

MSC extracellular vesicles rescue mitochondrial dysfunction and improve barrier integrity in clinically relevant models of ARDS

Johnatas Dutra Silva, Yue Su, Carolyn S Calfee, Kevin L Delucchi, Daniel Weiss, Danny F. McAuley, Cecilia O'Kane, Anna D. Krasnodembskaya

Please cite this article as: Silva JD, Su Y, Calfee CS, *et al*. MSC extracellular vesicles rescue mitochondrial dysfunction and improve barrier integrity in clinically relevant models of ARDS. *Eur Respir J* 2020; in press (https://doi.org/10.1183/13993003.02978-2020).

This manuscript has recently been accepted for publication in the *European Respiratory Journal*. It is published here in its accepted form prior to copyediting and typesetting by our production team. After these production processes are complete and the authors have approved the resulting proofs, the article will move to the latest issue of the ERJ online.

MSC extracellular vesicles rescue mitochondrial dysfunction and improve barrier integrity in clinically relevant models of ARDS

Johnatas Dutra Silva[1], Yue Su[1], Carolyn S Calfee[2], Kevin L Delucchi[3], Daniel Weiss[4], Danny F. McAuley[1], Cecilia O'Kane[1], Anna D. Krasnodembskaya[1]

1 Wellcome-Wolfson Institute for Experimental Medicine, School of Medicine, Dentistry, and Biomedical Sciences, Queen's University Belfast, Belfast, United Kingdom
2 Department of Medicine, Division of Pulmonary, Critical Care, Allergy and Sleep Medicine, University of California, San Francisco, San Francisco, CA, USA; Department of Anesthesia, University of California, San Francisco, San Francisco, CA, USA; Cardiovascular Research Institute, University of California, San Francisco, San Francisco, CA, USA.
3 Department of Psychiatry, University of California, San Francisco, San Francisco, CA, USA.
4 Department of Medicine, Larner College of Medicine, University of Vermont, Burlington, VT, USA

Corresponding author:

Correspondence and requests for reprints should be addressed to Anna D. Krasnodembskaya, B.Sc., M.Sc., Ph.D., Wellcome-Wolfson Institute for Experimental Medicine, School of Medicine, Dentistry and Biomedical Sciences, Queen's University Belfast, 97 Lisburn Road, Belfast BT9 7BL, UK. E-mail: a.krasnodembskaya@qub.ac.uk

Tweetable abstract:

We demonstrate that mitochondrial dysfunction is an important mechanism of ARDS pathogenesis. Mitochondrial transfer is crucial for the ability of MSC extracellular vesicles to restore integrity of the alveolar-capillary barrier.

Abstract (word count: 241)

Alveolar epithelial-capillary barrier disruption is a hallmark of Acute Respiratory Distress Syndrome (ARDS). Contribution of mitochondrial dysfunction to the compromised alveolar-capillary barrier in ARDS remains unclear. Mesenchymal stromal cells-derived extracellular vesicles (MSC EVs) are considered as a cell free therapy for ARDS. Mitochondrial transfer was shown to be important for the therapeutic effects of MSCs and MSC EVs. Here we investigated the contribution of mitochondrial dysfunction to the injury of alveolar epithelial and endothelial barriers in ARDS and the ability of MSC EVs to modulate alveolar-capillary barrier integrity through mitochondrial transfer.

Primary human small airway epithelial and pulmonary microvascular endothelial cells and human precision cut lung slices (PCLSs) were stimulated with endotoxin or plasma samples from patients with ARDS and treated with MSC EVs, barrier properties and mitochondrial functions were evaluated. LPS-injured mice were treated with MSC EVs and degree of lung injury and mitochondrial respiration of the lung tissue were assessed.

Inflammatory stimulation resulted in increased permeability coupled with pronounced mitochondrial dysfunction in both types of primary cells and PCLSs. EVs derived from normal MSCs restored barrier integrity and normal levels of oxidative phosphorylation while EV preparation which did not contain mitochondria was not effective. I*n vivo*, presence of mitochondria was critical for EV ability to reduce lung injury and restore mitochondrial respiration in the lung tissue.

In the ARDS environment MSC-EVs improve alveolar-capillary barrier properties through restoration of mitochondrial functions at least partially via mitochondrial transfer.

Introduction

ARDS is a life-threatening condition characterized by widespread uncontrolled inflammation in the lungs. Damage to the alveolar epithelial-endothelial barrier is a key aspect of ARDS pathophysiology implicated in development of oedema and diffuse alveolar damage (1, 2).

No specific pharmacological treatment is available for patients with ARDS, largely due to the heterogeneity of the underlying pathophysiological mechanisms in different subpopulations of patients (3, 4). Recently, two biological phenotypes have been identified retrospectively in four randomized clinical trials (5-7) and one observational study (8). These phenotypes had different clinical characteristics, biomarker profiles, clinical outcomes, and more importantly, they differently responded to interventions (positive end-expiratory pressure, fluid management strategy, low-dose macrolide therapy and simvastatin administration). Although the field is still waiting for the confirmation of these findings in prospective studies, when developing novel therapeutics, it will now be important to consider which ARDS phenotype is present and how it may respond.

Mitochondrial dysfunction and its potential mechanistic role in the pathophysiology of lung diseases such as COPD, asthma, pulmonary arterial hypertension, or idiopathic pulmonary fibrosis is increasingly recognised (9-11). Clinical observational data suggest that mitochondrial dysfunction has been associated with higher mortality in critically ill patients with sepsis (12) and survivors of the Multiple Organ Dysfunction Syndrome had better mitochondrial function with preservation of ATP and biogenesis markers (13). However, the role of mitochondrial dysfunction in the pathogenesis of ARDS is not sufficiently studied to date.

Mesenchymal stromal cells (MSCs) are being actively investigated as a potential therapy for ARDS. Accumulating evidence suggests that MSCs act primarily through their secretome,

key components of which are extracellular vesicles (EVs) (14,15). MSC EVs are being considered as a cell-free therapy for ARDS (16, 17). Several publications, including our own studies, have previously reported that MSC EVs contain mitochondria (18-21). Since the original finding by Spees et al (22), demonstrating that mitochondrial transfer from MSCs resulted in restoration of aerobic respiration in mitochondria-depleted A549ρ° cells, transfer of MSC-derived mitochondria to pulmonary epithelial cells has been associated with decreased inflammation and injury in the *in vivo* models of acute lung injury (18) and asthma (23). We have demonstrated that EV-mediated mitochondrial transfer was critical for MSC modulation of primary human macrophages (20). Furthermore, we have recently found that EV-mediated mitochondrial transfer is required for MSC ability to promote repair of human distal lung epithelial cells (21).

In this study we explored the contribution of mitochondrial dysfunction to the injury of alveolar epithelial and endothelial barriers in ARDS and the ability of MSC-EVs to modulate alveolar-capillary barrier functions through mitochondrial transfer. We hypothesized that the beneficial effect of MSC-EVs will depend on their ability to alleviate mitochondrial dysfunction and that EVs will have differential effects in the microenvironments of hypo- and hyper- inflammatory ARDS phenotypes. Some of the results of these studies were previously reported in the form of an abstract (24).

Methods

Detailed methods are described in Supplemental Methods.

Cell culture

Human Bone Marrow Mesenchymal Stromal Cells (MSCs) were from American Type Culture Collection (ATCC® PCS-500-012). These cells met all criteria set by the

International Society of Cellular Therapy for the definition of MSCs (25). Primary Human Pulmonary Microvascular Endothelial Cells (HPMECs) and Human Small Airway Epithelial Cells (HSAECs) were from PromoCell® (Heidelberg, Germany) and cultured according to manufacturer's instructions.

Generation of EVs from MSC with normal and dysfunctional mitochondria

MSC-EVs were isolated from MSC conditioned medium (CM) by ultracentrifugation according to Zhu et al (26) and characterized according to International Society for Extracellular Vesicles guidelines (27). To generate MSCs with dysfunctional mitochondria, MSCs were treated with 1µg/ml Rhodamine-6G (SigmaAldrich) for 48hrs [20] in medium supplemented with 50ug/ml uridine and 2.5mM sodium pyruvate (Sigma Aldrich) to support glycolysis, then washed with PBS and incubated for 48hrs in serum free medium. EVs were isolated from CM (Rho-EVs) and handled identically to EVs isolated from normal MSCs.

In Vivo LPS-induced Lung Injury Model

All animal experiments were approved by Animal Welfare Ethical Review Body of Queen's University Belfast, in accordance with UK Animals (Scientific Procedures) Act 1986. C57BL/6 male mice (8-12 w.o., Harlan Laboratories Ltd., UK) were used. Mice were anesthetized by xylazine/ketamine and LPS was instilled intratracheally (2mg/kg of body weight). 4hrs after injury, PBS, EVs or EVs-Rho were given via tail vein. 24hrs after injury, mice were euthanized and broncho-alveolar fluid (BALF) or lungs were taken for analysis or preparation of precision cut lung slices (mPCLSs).

Human Precision-Cut Lung Slices and Plasma Samples from ARDS Patients

Human lungs from organ donors (where the organ has been unsuitable for transplantation, and next of kin has consented for use in research) were used for lung slices cultured *ex vivo*. Ethical approval was given by National Review Ethics Service in association with NHS Blood and Transplant for lungs obtained within the UK (REC 14/LO/0250). Human PCLSs were prepared according to protocol by Uhl et al. (28). Plasma samples used in the study were from patients recruited to HARP-2 study (29). These samples were previously classified into 2 phenotypes based on concentrations of plasma inflammatory biomarkers (7). Only baseline samples obtained prior to intervention were used for experiments. 10 plasma samples representative of each phenotype were pooled and diluted in 1% complete medium to final concentration of 10% before use, plasma from healthy volunteers was used as a control. Ethical approval for use of patient samples for research was granted by the Office for Research Ethics Committees Northern Ireland.

Statistical Analysis

Statistical analysis was performed using Prism® 6 software (GraphPad Software, La Jolla, CA). Experiments were done at least in triplicate, the average of three technical replicates was taken as a single data point for each donor, and the points were pooled together for statistical analysis. Pooled data were presented as the mean with SD. For parametric data, Student's test or one-way analysis of variance with post hoc analysis using Bonferroni's selected comparisons were performed. For nonparametric data, Kruskal-Wallis test with post hoc analysis using Dunn's selected comparisons was used. The statistical significance level was set at $P < 0.05$.

Results

MSC EVs characterisation

EVs were isolated by ultracentrifugation from MSC CM generated by MSCs serum starved for 48hrs. Viability of MSCs after 48hrs of serum starvation was>90%. The dose of EVs used in the experiments was based on the final cell count of MSCs, which generated the conditioned medium (10µl per 1×10^6 cells). The protein and RNA concentrations of this dose of EVs were 98.32±34.6µg and 31.7±10.7ng, respectively (n=3).

Nanoparticle tracking analyses (NTA) demonstrated a particle size range of 100-700nm comprised of two populations of particles with sizes at 100-200nm corresponding to exosomes, 200-400nm corresponding to microvesicles, and substantial proportion of larger particles with the sizes at 500, 700nm and above falling into the size range of mitochondria (**Fig.1, A**). Consistently, fine structural analysis by electron microscopy showed presence of exosomes, multi-vesicular bodies and vesicles containing mitochondria (**Fig.1, B**). Western blotting of the EV pellet demonstrated pronounced expression of a mitochondrial marker, Translocase of Outer Membrane 20 (Tom20) protein (**Fig.1, C**). To further corroborate presence of mitochondria in the EV preparation, EVs were isolated from CM generated from MSCs pre-stained with Mitotracker Deep Red FM, incubated with beads conjugated with anti-CD44 or -CD63Ab and analysed by flow cytometry which demonstrated presence of vesicles double positive for MSC-derived mitochondria and surface markers for MSC EVs. Quantitatively, $CD44^+Mito^+$ EVs constituted 11.3±7.9% of the total EVs and $CD63^+Mito^+$ EVs constituted 17.6±11.7% of total EVs (**Fig.1, D**).

In a previous study, we have used Rhodamine-6G to induce specific irreversible inhibition of MSC mitochondrial function [19]. Importantly, this treatment does not affect MSC viability or capacity to secrete paracrine factors. Here we also tested if Rhodamine-6G treatment would affect MSC EV particle size distribution. NTA demonstrated that the size distribution profile and concentration of Rho-EVs was comparable to the profile of EVs isolated from control MSCs except that particles larger than 400nm, corresponding to the size range of

mitochondria, were absent (**Fig. 1,E**). Consistently, Western Blot analysis of Rho-EVs did not detect presence of TOM20 protein (**Fig.1,F**). Rho-EVs were used in all the subsequent experiments to investigate the contribution of mitochondria to the overall EV effect.

EV mitochondria are readily internalised by HSAECs and HPMECs and restore barrier integrity disrupted by LPS

Mitochondrial uptake from MSC EVs by pulmonary cells was visualised by Nikon Eclipse Ti-E microscopy. EVs were isolated from MSC pre-treated with Mitotracker Deep Red FM and co-cultured with HSAECs or HPMECs that were pre-stained with Mitotracker Green to visualise endogenous mitochondria (**Fig.2, A-C**). 3D reconstruction of multiple z-stacks and deconvolution of images were done using Nikon 6D Eclipse software. At 24 hrs, there was evidence of robust uptake of MSC-derived mitochondria by both epithelial and endothelial cells (**Suppl. Videos 1, 2**).

As expected, in both HSAECs and HPMECs, LPS stimulation resulted in significant upregulation of IL-8 production. This effect was significantly reversed by both types of EVs (**Fig.2, D-E**), indicating that mitochondrial transfer is not critical for EV effects on IL-8 production.

LPS stimulation also resulted in significant disruption of both epithelial and endothelial cell barriers as indicated by the alterations in the electrical impedance of the cell monolayer (**Fig.2, F-I**). In both cell types, control MSC-EVs were able to restore barrier integrity while Rho-EVs had no effect.

LPS induces mitochondrial dysfunction in HSAECs and HPMECs which is alleviated by EV mitochondria

LPS induced marked decrease in the mitochondrial membrane potential (measured as a ratio between red and green JC-1 dye fluorescence) in both cell types (**Fig.3 A-C**). This was accompanied by significant upregulation of the mitochondrial Reactive Oxygen Species (mtROS), (**Fig.3 D-F**), collectively demonstrating LPS-induced mitochondrial dysfunction.

EVs were able to partially restore these parameters in both cell types and this effect was dependant on the presence of mitochondria, as Rho-EVs did not have any effect (**Fig. 3, A-F**).

These findings were further corroborated by assessment of the mitochondrial respiration by measurements of cell oxygen consumption rate, LPS significantly reduced basal and maximum mitochondrial respiration and ATP turnover in both cell types, these effects were partially reversed by control EVs but not Rho-EVs (**Fig.3, G-N**).

MSC EVs reverse LPS-induced changes in mitochondrial quality control mechanisms in HSAECS and HPMECs

To evaluate effects on mitochondrial homeostasis we assessed levels of mitophagy and mitochondrial biogenesis in epithelial and endothelial cells. Mitophagy was assessed by quantification of co-localisation of mitochondria (Mitotracker Red) to autophagosomes (LC3-II lysosomal marker, green) using confocal microscopy. LPS stimulation induced significant upregulation in the levels of mitophagy in both cell types which were restored to normal levels by MSC-EVs (**Fig.4, A-C**).

Mitochondrial biogenesis was assessed by measurements of mtDNA replication levels using BrdU incorporation assay (30). As opposed to mitophagy, levels of mitochondria biogenesis were significantly inhibited by LPS in HSAECS and treatment with MSC-EVs resulted in restoration of the normal levels of mtDNA replication (**Fig. 4, D,E**). In HPMECs, although changes in biogenesis levels followed the same trend, effects did not reach statistical significance (**Fig.4, D,F**).

MSC EVs downregulate LPS-induced inflammatory response and attenuate mitochondrial dysfunction in human PCLSs

Next, we investigated the effects of EVs on LPS-induced mitochondrial dysfunction in the more physiologically relevant human lung tissue model. Human precision cut lung slices (PCLSs) were exposed to LPS and treated with EVs for 24 hrs. Mitochondrial transfer to PCLSs was visualised by confocal microscopy (**Suppl. Figure 1**). LPS stimulation resulted in significant upregulation of IL-8 and TNF-α secretion levels in PCLS conditioned medium, which were significantly alleviated by control EVs but not Rho-EVs (**Fig.5, A,B**). LPS also induced significant upregulation of the Receptor for Advanced Glycation End Products (RAGE) levels indicating alveolar epithelial injury [30]. Addition of control but not Rho-EVs restored RAGE levels to the baseline (**Fig.5, C**). Importantly, LPS stimulation did not induce cell death (as measured by LDH release) suggesting that observed changes in cytokine secretion were not accountable to passive leakage from necrotic cells (**Fig.5, D**). Addition of a specific mtROS inhibitor, MitoTempo, resulted in downregulation of TNF-α, IL-8 and RAGE secretion recapitulating the effect of control EVs, suggesting that inhibition of mtROS may be partially responsible for the anti-inflammatory effect of EV mitochondrial transfer (**Fig.5, A-D**).

Exposure of PCLSs to LPS for 24hrs induced significant depolarisation of the mitochondrial membrane potential and upregulation of mtROS. Both of these endpoints were restored by administration of control EVs but not Rho-EVs (**Fig.5, E-H**). Consistently, analysis of PCLS oxygen consumption rate demonstrated LPS-induced inhibition of basal and maximal mitochondrial respiration and ATP turnover. Addition of control but not Rho-EVs was able to restore mitochondrial respiration (**Fig.5, I-L**). Treatment with MitoTempo did not have significant effect on restoration of mitochondrial respiration in PCLSs suggesting that

inhibition of mtROS alone is not enough to alleviate LPS-induced mitochondrial dysfunction at the lung tissue level.

MSC EVs modulate barrier properties and inflammatory response of the HSAECS and HPMECs when stimulated with plasma samples from patients with ARDS. Hypo-inflammatory ARDS environment is more responsive to the EV treatment.

To mimic human ARDS environment more closely and to investigate EV effects in the different ARDS phenotypes, HSAECs and HPMECs were cultured for 24 hours in the presence of 10% plasma samples of patients with ARDS previously classified into hypo- or hyper-inflammatory phenotypes (7).

Exposure to both types of plasma samples elicited comparable increases in IL-8 secretion in both epithelial and endothelial cells. Addition of both control and Rho-EVs comparably reduced ARDS plasma-stimulated increases (**Fig.6, A,B**). Addition of MitoTempo resulted in strong inhibition of IL-8 secretion in both cell types and both ARDS phenotypes.

Assessment of the barrier function demonstrated that exposure to each type of ARDS plasma induced comparable disruption of the barrier integrity in HSAECs and HPMECs (**Fig.6, C-J**). This was partially restored by EVs only in the case of hypo-inflammatory plasma, Rho-EVs had no effect (**Fig.6, C-F**).

Exposure to both types of ARDS plasma significantly impaired mitochondrial ATP turnover in HSAECs and HPMECs **(Fig.6, K,L)**. In both cell types, MSC-EVs were able to significantly attenuate defects in the mitochondrial respiration in the presence of hypo-inflammatory plasma, whereas in hyper-inflammatory plasma EV effect was partial or absent. Rho-EVs did not have any effect on the mitochondrial respiration. Treatment with MitoTempo was not able to significantly improve mitochondrial ATP turnover (**Fig.6, K,L**).

Angiopoietin-2 (Ang-2) is a well recognised mediator and biomarker of pulmonary and systemic vascular injury (31-33). Plasma concentrations of Ang-2 have important predictive value for the development of ARDS and robustly predict poor clinical outcomes in adults and children with ARDS (34, 35). Importantly, statistically significant decrease in plasma Ang-2 concentrations at 6 hrs after MSC infusion was reported in the START study (a randomised phase 2a safety trial of MSCs in ARDS) (36). Therefore, we were interested in the effects of EVs on Ang-2 secretion levels by endothelial and epithelial cells in our models. LPS stimulation resulted in robust upregulation of Ang-2 secretion by both HPMECs and SAECs (of note, SAECs had numerically almost 10-fold lower levels of Ang-2 secretion compared to HPMECs), this was partially restored by control EVs and MitoTempo but not Rho-EVs (**Fig. 7A,B**). Consistently, stimulation with ARDS plasma also elicited an increase in Ang-2 secretion by both cell types. In HPMECs control EVs but not Rho-EVs were able to partially reduce its levels in the presence of hypo-inflammatory plasma whereas no effect was detected in the presence of hyper-inflammatory plasma (**Fig. 7C).** In SAECs, control EVs but not Rho-EVs were able to partially restore Ang-2 levels in the presence of hypo-inflammatory plasma whereas addition of both control and Rho-EVs comparably reduced Ang-2 concentrations in the presence of hyper-inflammatory plasma **(Fig. 7D).**

MSC-EVs attenuate lung injury and restore lung tissue mitochondrial respiration in the mouse model of LPS-induced lung injury

Given the above results, we hypothesized that EV-mediated mitochondrial transfer would improve mitochondrial dysfunction in an *in vivo* lung injury model. Effects of 2 different EV doses were compared: EVs generated from $5x10^5$ and $1x10^6$ MSCs. Administration of either dose of control EVs comparably decreased the LPS-stimulated increases in BALF total protein**,** total and differential cell counts, (**Fig. 8, A-D**) Administration of Rho-EVs

(generated from $1x10^6$ MSCs) had no effect. Cytospin preparations of BALF demonstrated substantial inflammatory cell recruitment to the alveolar compartment, consisting predominantly of neutrophils, in the LPS-injured group which was reduced by administration of EVs but not Rho-EVs (**Fig.8, E**).

EV but not Rho-EV treatment demonstrated a trend towards reduction of BALF levels of representative inflammatory cytokines (TNF-α and KC) however the effect did not reach statistical significance (**Fig.8, F,G)**

To assess mitochondrial function, we measured mitochondrial respiration in the mouse lung tissue in this model using PCLSs (**Fig.8, H**). LPS-induced injury resulted in significant downregulation of basal and maximal mitochondrial respiration and of mitochondrial ATP turnover. Systemic administration of both doses of control EVs but not Rho-EVs restored both mitochondrial respiration and ATP production **(Fig. 8, I-L)**.

Discussion

The major findings from this study are the following: 1) MSC-EVs contain mitochondria, which are readily internalised by recipient cells and intercalate into the endogenous mitochondrial network (**Fig. 1,2**); 2) LPS-induced inflammatory response and increase in the epithelial and endothelial barrier permeability coupled with significant mitochondrial dysfunction. The transfer of mitochondria in MSC-EVs was crucial not only for the alleviation of mitochondrial dysfunction but also for the restoration of barrier integrity in both cells types, suggesting important role of mitochondria in the maintenance of alveolar-capillary barrier function (**Fig. 2,3**). 3) In both cell types, MSC-EVs were able to restore normal levels of mitophagy and mitochondrial biogenesis, which were perturbed by LPS (**Fig.4**) 4) MSC-EVs mitochondrial transfer was able to attenuate mitochondrial dysfunction and restore mitochondrial respiration inhibited by LPS at the lung tissue level in PCLSs (**Fig.5**); 5)

Stimulation with ARDS plasma significantly impaired barrier integrity and mitochondrial function in both epithelial and endothelial cells, however therapeutic effect of MSC-EVs was only seen in the presence of plasma from patients with hypo-inflammatory phenotype **(Figs.6,7**); 6) Therapeutic effect of MSC-EVs in the *in vivo* model of LPS-induced lung injury was dependent on the presence of mitochondria and EV mitochondrial transfer improved mitochondrial respiration in the lung tissue *in vivo* (**Fig.8**).

Once questioned on the reality of their existence, MSC extracellular vesicles are now entering clinical arena as a potent alternative to the whole-cell therapy (16, 37, 38). Islam et al (18) was the first to report that MSC-EVs could act as vehicles to transfer functional mitochondria and restore bioenergetics of the host cells, compromised by inflammatory microenvironment. This was followed by a seminal publication by Phinney et al (19), demonstrating that MSCs actively secrete mitochondria into EVs, as a result of unfinished mitophagy. We have previously reported that mitochondrial transfer is important for MSC modulation of macrophages leading to their metabolic reprogramming towards anti-inflammatory phenotype and also promote wound healing capacity of human small airway epithelial cells (20, 21, 39). Notably, recent publication reports that monocytes also are capable of mitochondrial secretion in the EVs and that mitochondrial stress contributes to the inflammatory properties of their secretome (40). Here we provide characterisation of the mitochondria present in the MSC-EVs by a range of techniques (**Fig.1**). We demonstrate presence of vesicles larger than 400nm which are not accountable for apoptotic bodies and possessing ultrastructural characteristics of mitochondria, presence of vesicles double-positive for MSC mitochondria and MSC-EV surface markers CD44 and CD63, and high level of expression of mitochondrial outer membrane protein in the EVs (**Fig.1 A-D**). Importantly, we demonstrate that MSCs which mitochondria were rendered dysfunctional by pre-treatment with Rhodamine-6G (20) also secrete EVs and their concentration and size distribution profiles are comparable with

EVs secreted by normal MSC, except for the absence of vesicles above 400nm in size, corresponding to the mitochondria (**Fig.1, E**).

Accumulating evidence indicate that alterations in the mitochondrial function play a role in development of many forms of critical illness (13, 41, 42). However, the data on contribution of mitochondrial dysfunction to the disruption of the alveolar-capillary barrier in ARDS are limited. Islam and colleagues (18) were the first to consider that MSC therapeutic effect in lung injury is mediated through restoration of mitochondrial bioenergetics and ATP production of alveolar epithelial cells. Recent publication from the same group determined mechanistic links between mitochondrial dysfunction and microvascular hyperpermeability *in vivo* (43). Here we demonstrate that LPS stimulation results in significant impairment of barrier integrity of primary human small airway epithelial and microvascular endothelial cells which is coupled with profound mitochondrial dysfunction and disturbance of mitochondrial biogenesis and mitophagy (**Fig 3,4**). Donation of the exogenous mitochondria results in the restoration of normal mitochondrial respiration in both cell types to the normal levels and is critical for the therapeutic effect of EVs on recovery of the epithelial and endothelial barrier functions.

In line with these findings we observe that LPS stimulation impairs mitochondrial membrane potential, increases mtROS production and inhibits mitochondrial respiration in the human PCLSs, and mitochondrial transfer from MSC-EVs is crucial to alleviate mitochondrial dysfunction and restore mitochondrial respiration in this model (**Fig.5**).

Overproduction of mtROS is thought to be crucial factor in the development of mitochondrial dysfunction leading to disruption of mitochondrial membrane integrity, dissipation of $\Delta\Psi$ and further damage to the cell (44-46). Antioxidant-based therapies are explored for clinical efficacy in multiple disease conditions including critical illness (47-49). Interestingly, treatment with mitochondrial ROS inhibitor, MitoTempo, was sufficient to reverse

inflammatory response but was not able to restore mitochondrial respiration (**Fig.5,6**), suggesting that MSC-EVs effect cannot be fully explained by inhibition of mtROS production. It is plausible to hypothesise that upregulation of mitochondrial biogenesis observed with EV mitochondrial transfer could be important for alleviation of LPS-induced mitochondrial dysfunction.

Two biological subphenotypes of ARDS (hypo- and hyper-inflammatory) are retrospectively identified in 4 large clinical trials, including HARP-2 (7). Interestingly, subsequent study using microarray analysis of whole-blood gene expression in an observational cohort of 210 patients with sepsis-related ARDS found that one-third of genes was differentially expressed between phenotypes and patients in the "reactive" or "hyper-inflammed" group were characterised by expression of genes indicative of mitochondrial dysfunction (50). We found that stimulation of epithelial as well as endothelial cells with ARDS plasma induces inhibition of mitochondrial respiration regardless of the phenotype (**Fig. 6**). MSC-EVs however were able to partially restore both mitochondrial function and barrier integrity only in hypo-inflammatory plasma and presence of mitochondria was central to this effect (**Fig. 6**), suggesting, that patients with hypo-inflammatory phenotype may be more responsive to the MSC-EVs treatment. It is plausible that in the setting of hyper-inflammatory microenvironment there is a threshold to endothelial and epithelial cell injury, beyond which retrieval of physiological bioenergetic function is hindered.

Ang-2 has been established as a key mediator and biomarker of endothelial injury in ARDS (31-35) and was the single biomarker which levels were significantly reduced after MSC administration in the START study (36). It is important to highlight that in the present study control but not Rho-EVs demonstrated strong trend towards reduction of Ang-2 secretion levels by both HPMECS and SAECS in the presence of LPS and ARDS plasma, indicating

relevance of EV mitochondrial transfer for alleviation of the severity of endothelial injury (**Fig. 7**).

To confirm the importance of MSC-EVs mitochondrial transfer in the lung injury *in vivo*, endotoxin-injured mice were given EVs derived from normal or Rhodamine-6G-treated MSCs. Normal EV, but not Rho-EVs, were able to significantly reduce the extent of lung injury after 24 hours (**Fig.8**). These data are in line with several previously published reports demonstrating therapeutic effects of MSC-EVs in the *in vivo* models of ARDS (26, 51-55). Furthermore, measurements of oxygen consumption rates of the lung tissue in this model using mPCLSs, demonstrated that instillation of endotoxin significantly inhibited mitochondrial respiration and ATP production in the mouse lungs and EV mitochondrial transfer was able to restore mitochondrial respiration to normal levels (**Fig.8).**

This study has limitations. We used ARDS plasma diluted to 10% by volume; while exposing cells to all constituents of the ARDS microenvironment, this effectively reduced the concentrations of the stimuli. We acknowledge that BALF would be more suitable environment to stimulate epithelial cells, unfortunately BALF samples from both phenotypes were not available. The endotoxin-induced lung injury model is relatively mild and does not reflect complexity of human ARDS; the primary aim of the *in vivo* experiments was to provide a proof of principle that MSC EVs are capable to alleviate mitochondrial dysfunction *in vivo*. Additionally, we did not investigate molecular mechanisms by which mitochondria in EVs are protective in lung injury and specifically molecular mechanisms responsible for alleviation of endothelial barrier dysfunction, this is the subject of ongoing work. We did not use fibroblasts- derived EVs as cell specific control for *in vivo* experiments, however previous studies have demonstrated that fibroblast-derived EVs had no therapeutic effects in LPS and *E.coli*-induced murine lung injury models (55, 56). Our primary focus in this study was to investigate the mechanistic role of MSC EV mediated mitochondrial transfer, therefore we

used Rho-EVs which contain similar profile of vesicles but lack mitochondria, we believe this would constitute a better control.

In conclusion, we for the first time, have demonstrated that ARDS environment induces significant mitochondrial dysfunction in human lung tissue implicated in the impairment of alveolar-capillary barrier functions. Therapeutic effect of MSC EVs on the restoration of barrier integrity is mediated by mitochondrial transfer.

Acknowledgements

This work was supported by UK Medical Research Council Research Awards (MRC MR/R025096/1 and MR/S009426/1 – to AK). We thank Dr Ileana Micu for technical assistance with imaging work, Dr John Conlon for technical assistance with processing of clinical samples, Dr Ke Xu and Mr David Butler for general technical support.

References

1. Huppert LA, Matthay MA, Ware LB. Pathogenesis of Acute Respiratory Distress Syndrome. *Semin Respir Crit Care Med* 2019; 40: 31-39.
2. Matthay MA, Zemans RL, Zimmerman GA, Arabi YM, Beitler JR, Mercat A, Herridge M, Randolph AG, Calfee CS. Acute respiratory distress syndrome. *Nat Rev Dis Primers* 2019; 5: 18.

3. Lewis SR, Pritchard MW, Thomas CM, Smith AF. Pharmacological agents for adults with acute respiratory distress syndrome. *Cochrane Database Syst Rev* 2019; 7: CD004477.
4. Laffey JG, Kavanagh BP. Negative trials in critical care: why most research is probably wrong. *Lancet Respir Med* 2018; 6: 659-660.
5. Calfee CS, Delucchi K, Parsons PE, Thompson BT, Ware LB, Matthay MA, Network NA. Subphenotypes in acute respiratory distress syndrome: latent class analysis of data from two randomised controlled trials. *Lancet Respir Med* 2014; 2: 611-620.
6. Famous KR, Delucchi K, Ware LB, Kangelaris KN, Liu KD, Thompson BT, Calfee CS, Network A. Acute Respiratory Distress Syndrome Subphenotypes Respond Differently to Randomized Fluid Management Strategy. *Am J Respir Crit Care Med* 2017; 195: 331-338.
7. Calfee CS, Delucchi KL, Sinha P, Matthay MA, Hackett J, Shankar-Hari M, McDowell C, Laffey JG, O'Kane CM, McAuley DF, Irish Critical Care Trials G. Acute respiratory distress syndrome subphenotypes and differential response to simvastatin: secondary analysis of a randomised controlled trial. *Lancet Respir Med* 2018; 6: 691-698.
8. Bos LD, Schouten LR, van Vught LA, Wiewel MA, Ong DSY, Cremer O, Artigas A, Martin-Loeches I, Hoogendijk AJ, van der Poll T, Horn J, Juffermans N, Calfee CS, Schultz MJ, consortium M. Identification and validation of distinct biological phenotypes in patients with acute respiratory distress syndrome by cluster analysis. *Thorax* 2017; 72: 876-883.
9. Riou M, Alfatni A, Charles AL, Andres E, Pistea C, Charloux A, Geny B. New Insights into the Implication of Mitochondrial Dysfunction in Tissue, Peripheral Blood Mononuclear Cells, and Platelets during Lung Diseases. *J Clin Med* 2020; 9.
10. Ryter SW, Rosas IO, Owen CA, Martinez FJ, Choi ME, Lee CG, Elias JA, Choi AMK. Mitochondrial Dysfunction as a Pathogenic Mediator of Chronic Obstructive

Pulmonary Disease and Idiopathic Pulmonary Fibrosis. *Ann Am Thorac Soc* 2018; 15: S266-S272.

11. Cho HY, Kleeberger SR. Mitochondrial biology in airway pathogenesis and the role of NRF2. *Arch Pharm Res* 2020; 43: 297-320.
12. Brealey D, Brand M, Hargreaves I, Heales S, Land J, Smolenski R, Davies NA, Cooper CE, Singer M. Association between mitochondrial dysfunction and severity and outcome of septic shock. *Lancet* 2002; 360: 219-223.
13. Carre JE, Orban JC, Re L, Felsmann K, Iffert W, Bauer M, Suliman HB, Piantadosi CA, Mayhew TM, Breen P, Stotz M, Singer M. Survival in critical illness is associated with early activation of mitochondrial biogenesis. *Am J Respir Crit Care Med* 2010; 182: 745-751.
14. Phinney DG, Pittenger MF. Concise Review: MSC-Derived Exosomes for Cell-Free Therapy. *Stem Cells* 2017; 35: 851-858.
15. Elahi FM, Farwell DG, Nolta JA, Anderson JD. Preclinical translation of exosomes derived from mesenchymal stem/stromal cells. *Stem Cells* 2020; 38: 15-21.
16. Abraham A, Krasnodembskaya A. Mesenchymal stem cell-derived extracellular vesicles for the treatment of acute respiratory distress syndrome. *Stem Cells Transl Med* 2020; 9: 28-38.
17. Mahida RY, Matsumoto S, Matthay MA. Extracellular Vesicles: A New Frontier for Research in Acute Respiratory Distress Syndrome. *Am J Respir Cell Mol Biol* 2020; 63: 15-24.
18. Islam MN, Das SR, Emin MT, Wei M, Sun L, Westphalen K, Rowlands DJ, Quadri SK, Bhattacharya S, Bhattacharya J. Mitochondrial transfer from bone-marrow-derived stromal cells to pulmonary alveoli protects against acute lung injury. *Nat Med* 2012; 18: 759-765.

19. Phinney DG, Di Giuseppe M, Njah J, Sala E, Shiva S, St Croix CM, Stolz DB, Watkins SC, Di YP, Leikauf GD, Kolls J, Riches DW, Deiuliis G, Kaminski N, Boregowda SV, McKenna DH, Ortiz LA. Mesenchymal stem cells use extracellular vesicles to outsource mitophagy and shuttle microRNAs. *Nat Commun* 2015; 6: 8472.

20. Morrison TJ, Jackson MV, Cunningham EK, Kissenpfennig A, McAuley DF, O'Kane CM, Krasnodembskaya AD. Mesenchymal Stromal Cells Modulate Macrophages in Clinically Relevant Lung Injury Models by Extracellular Vesicle Mitochondrial Transfer. *Am J Respir Crit Care Med* 2017; 196: 1275-1286.

21. Fergie N, Todd N, McClements L, McAuley D, O'Kane C, Krasnodembskaya A. Hypercapnic acidosis induces mitochondrial dysfunction and impairs the ability of mesenchymal stem cells to promote distal lung epithelial repair. *FASEB J* 2019; 33: 5585-5598.

22. Spees JL, Olson SD, Ylostalo J, Lynch PJ, Smith J, Perry A, Peister A, Wang MY, Prockop DJ. Differentiation, cell fusion, and nuclear fusion during ex vivo repair of epithelium by human adult stem cells from bone marrow stroma. *Proc Natl Acad Sci U S A* 2003; 100: 2397-2402.

23. Ahmad T, Mukherjee S, Pattnaik B, Kumar M, Singh S, Kumar M, Rehman R, Tiwari BK, Jha KA, Barhanpurkar AP, Wani MR, Roy SS, Mabalirajan U, Ghosh B, Agrawal A. Miro1 regulates intercellular mitochondrial transport & enhances mesenchymal stem cell rescue efficacy. *EMBO J* 2014; 33: 994-1010.

24. Silva JD, Su Y, McAuley DF, O'Kane C, Krasnodembskaya A. Transfer of mitochondria through msc-derived extracellular vesicles improves alveolar-capillary barrier integrity and alleviate mitochondrial dysfunction in acute respiratory distress syndrome (ards). *Cytotherapy* 2020; VOLUME 22: S25.

25. Dominici M, Le Blanc K, Mueller I, Slaper-Cortenbach I, Marini F, Krause D, Deans R, Keating A, Prockop D, Horwitz E. Minimal criteria for defining multipotent mesenchymal stromal cells. The International Society for Cellular Therapy position statement. *Cytotherapy* 2006; 8: 315-317.

26. Zhu YG, Feng XM, Abbott J, Fang XH, Hao Q, Monsel A, Qu JM, Matthay MA, Lee JW. Human mesenchymal stem cell microvesicles for treatment of Escherichia coli endotoxin-induced acute lung injury in mice. *Stem Cells* 2014; 32: 116-125.

27. Thery C, Witwer KW, Aikawa E, Alcaraz MJ, Anderson JD, Andriantsitohaina R, Antoniou A, Arab T, Archer F, Atkin-Smith GK, Ayre DC, Bach JM, Bachurski D, Baharvand H, Balaj L, Baldacchino S, Bauer NN, Baxter AA, Bebawy M, Beckham C, Bedina Zavec A, Benmoussa A, Berardi AC, Bergese P, Bielska E, Blenkiron C, Bobis-Wozowicz S, Boilard E, Boireau W, Bongiovanni A, Borras FE, Bosch S, Boulanger CM, Breakefield X, Breglio AM, Brennan MA, Brigstock DR, Brisson A, Broekman ML, Bromberg JF, Bryl-Gorecka P, Buch S, Buck AH, Burger D, Busatto S, Buschmann D, Bussolati B, Buzas EI, Byrd JB, Camussi G, Carter DR, Caruso S, Chamley LW, Chang YT, Chen C, Chen S, Cheng L, Chin AR, Clayton A, Clerici SP, Cocks A, Cocucci E, Coffey RJ, Cordeiro-da-Silva A, Couch Y, Coumans FA, Coyle B, Crescitelli R, Criado MF, D'Souza-Schorey C, Das S, Datta Chaudhuri A, de Candia P, De Santana EF, De Wever O, Del Portillo HA, Demaret T, Deville S, Devitt A, Dhondt B, Di Vizio D, Dieterich LC, Dolo V, Dominguez Rubio AP, Dominici M, Dourado MR, Driedonks TA, Duarte FV, Duncan HM, Eichenberger RM, Ekstrom K, El Andaloussi S, Elie-Caille C, Erdbrugger U, Falcon-Perez JM, Fatima F, Fish JE, Flores-Bellver M, Forsonits A, Frelet-Barrand A, Fricke F, Fuhrmann G, Gabrielsson S, Gamez-Valero A, Gardiner C, Gartner K, Gaudin R, Gho YS, Giebel B, Gilbert C, Gimona M, Giusti I, Goberdhan DC, Gorgens A, Gorski SM, Greening DW, Gross JC,

Gualerzi A, Gupta GN, Gustafson D, Handberg A, Haraszti RA, Harrison P, Hegyesi H, Hendrix A, Hill AF, Hochberg FH, Hoffmann KF, Holder B, Holthofer H, Hosseinkhani B, Hu G, Huang Y, Huber V, Hunt S, Ibrahim AG, Ikezu T, Inal JM, Isin M, Ivanova A, Jackson HK, Jacobsen S, Jay SM, Jayachandran M, Jenster G, Jiang L, Johnson SM, Jones JC, Jong A, Jovanovic-Talisman T, Jung S, Kalluri R, Kano SI, Kaur S, Kawamura Y, Keller ET, Khamari D, Khomyakova E, Khvorova A, Kierulf P, Kim KP, Kislinger T, Klingeborn M, Klinke DJ, 2nd, Kornek M, Kosanovic MM, Kovacs AF, Kramer-Albers EM, Krasemann S, Krause M, Kurochkin IV, Kusuma GD, Kuypers S, Laitinen S, Langevin SM, Languino LR, Lannigan J, Lasser C, Laurent LC, Lavieu G, Lazaro-Ibanez E, Le Lay S, Lee MS, Lee YXF, Lemos DS, Lenassi M, Leszczynska A, Li IT, Liao K, Libregts SF, Ligeti E, Lim R, Lim SK, Line A, Linnemannstons K, Llorente A, Lombard CA, Lorenowicz MJ, Lorincz AM, Lotvall J, Lovett J, Lowry MC, Loyer X, Lu Q, Lukomska B, Lunavat TR, Maas SL, Malhi H, Marcilla A, Mariani J, Mariscal J, Martens-Uzunova ES, Martin-Jaular L, Martinez MC, Martins VR, Mathieu M, Mathivanan S, Maugeri M, McGinnis LK, McVey MJ, Meckes DG, Jr., Meehan KL, Mertens I, Minciacchi VR, Moller A, Moller Jorgensen M, Morales-Kastresana A, Morhayim J, Mullier F, Muraca M, Musante L, Mussack V, Muth DC, Myburgh KH, Najrana T, Nawaz M, Nazarenko I, Nejsum P, Neri C, Neri T, Nieuwland R, Nimrichter L, Nolan JP, Nolte-'t Hoen EN, Noren Hooten N, O'Driscoll L, O'Grady T, O'Loghlen A, Ochiya T, Olivier M, Ortiz A, Ortiz LA, Osteikoetxea X, Ostergaard O, Ostrowski M, Park J, Pegtel DM, Peinado H, Perut F, Pfaffl MW, Phinney DG, Pieters BC, Pink RC, Pisetsky DS, Pogge von Strandmann E, Polakovicova I, Poon IK, Powell BH, Prada I, Pulliam L, Quesenberry P, Radeghieri A, Raffai RL, Raimondo S, Rak J, Ramirez MI, Raposo G, Rayyan MS, Regev-Rudzki N, Ricklefs FL, Robbins PD, Roberts DD, Rodrigues SC, Rohde E,

Rome S, Rouschop KM, Rughetti A, Russell AE, Saa P, Sahoo S, Salas-Huenuleo E, Sanchez C, Saugstad JA, Saul MJ, Schiffelers RM, Schneider R, Schoyen TH, Scott A, Shahaj E, Sharma S, Shatnyeva O, Shekari F, Shelke GV, Shetty AK, Shiba K, Siljander PR, Silva AM, Skowronek A, Snyder OL, 2nd, Soares RP, Sodar BW, Soekmadji C, Sotillo J, Stahl PD, Stoorvogel W, Stott SL, Strasser EF, Swift S, Tahara H, Tewari M, Timms K, Tiwari S, Tixeira R, Tkach M, Toh WS, Tomasini R, Torrecilhas AC, Tosar JP, Toxavidis V, Urbanelli L, Vader P, van Balkom BW, van der Grein SG, Van Deun J, van Herwijnen MJ, Van Keuren-Jensen K, van Niel G, van Royen ME, van Wijnen AJ, Vasconcelos MH, Vechetti IJ, Jr., Veit TD, Vella LJ, Velot E, Verweij FJ, Vestad B, Vinas JL, Visnovitz T, Vukman KV, Wahlgren J, Watson DC, Wauben MH, Weaver A, Webber JP, Weber V, Wehman AM, Weiss DJ, Welsh JA, Wendt S, Wheelock AM, Wiener Z, Witte L, Wolfram J, Xagorari A, Xander P, Xu J, Yan X, Yanez-Mo M, Yin H, Yuana Y, Zappulli V, Zarubova J, Zekas V, Zhang JY, Zhao Z, Zheng L, Zheutlin AR, Zickler AM, Zimmermann P, Zivkovic AM, Zocco D, Zuba-Surma EK. Minimal information for studies of extracellular vesicles 2018 (MISEV2018): a position statement of the International Society for Extracellular Vesicles and update of the MISEV2014 guidelines. *J Extracell Vesicles* 2018; 7: 1535750.

28. Uhl FE, Vierkotten S, Wagner DE, Burgstaller G, Costa R, Koch I, Lindner M, Meiners S, Eickelberg O, Konigshoff M. Preclinical validation and imaging of Wnt-induced repair in human 3D lung tissue cultures. *Eur Respir J* 2015; 46: 1150-1166.

29. McAuley DF, Laffey JG, O'Kane CM, Perkins GD, Mullan B, Trinder TJ, Johnston P, Hopkins PA, Johnston AJ, McDowell C, McNally C, Investigators H-, Irish Critical Care Trials G. Simvastatin in the acute respiratory distress syndrome. *N Engl J Med* 2014; 371: 1695-1703.

30. Lentz SI, Edwards JL, Backus C, McLean LL, Haines KM, Feldman EL. Mitochondrial DNA (mtDNA) biogenesis: visualization and duel incorporation of BrdU and EdU into newly synthesized mtDNA in vitro. *J Histochem Cytochem* 2010; 58: 207-218.

31. Bhandari V, Choo-Wing R, Lee CG, Zhu Z, Nedrelow JH, Chupp GL, Zhang X, Matthay MA, Ware LB, Homer RJ, Lee PJ, Geick A, de Fougerolles AR, Elias JA. Hyperoxia causes angiopoietin 2-mediated acute lung injury and necrotic cell death. *Nat Med* 2006; 12: 1286-1293.

32. Parikh SM. Angiopoietins and Tie2 in vascular inflammation. *Curr Opin Hematol* 2017; 24: 432-438.

33. Agrawal A, Matthay MA, Kangelaris KN, Stein J, Chu JC, Imp BM, Cortez A, Abbott J, Liu KD, Calfee CS. Plasma angiopoietin-2 predicts the onset of acute lung injury in critically ill patients. *Am J Respir Crit Care Med* 2013; 187: 736-742.

34. Calfee CS, Gallagher D, Abbott J, Thompson BT, Matthay MA, Network NA. Plasma angiopoietin-2 in clinical acute lung injury: prognostic and pathogenetic significance. *Crit Care Med* 2012; 40: 1731-1737.

35. Zinter MS, Spicer A, Orwoll BO, Alkhouli M, Dvorak CC, Calfee CS, Matthay MA, Sapru A. Plasma angiopoietin-2 outperforms other markers of endothelial injury in prognosticating pediatric ARDS mortality. *Am J Physiol Lung Cell Mol Physiol* 2016; 310: L224-231.

36. Matthay MA, Calfee CS, Zhuo H, Thompson BT, Wilson JG, Levitt JE, Rogers AJ, Gotts JE, Wiener-Kronish JP, Bajwa EK, Donahoe MP, McVerry BJ, Ortiz LA, Exline M, Christman JW, Abbott J, Delucchi KL, Caballero L, McMillan M, McKenna DH, Liu KD. Treatment with allogeneic mesenchymal stromal cells for moderate to severe acute respiratory distress syndrome (START study): a randomised phase 2a safety trial. *Lancet Respir Med* 2019; 7: 154-162.

37. Wiklander OPB, Brennan MA, Lotvall J, Breakefield XO, El Andaloussi S. Advances in therapeutic applications of extracellular vesicles. *Sci Transl Med* 2019; 11.

38. Lee JH, Park J, Lee JW. Therapeutic use of mesenchymal stem cell-derived extracellular vesicles in acute lung injury. *Transfusion* 2019; 59: 876-883.

39. Jackson MV, Morrison TJ, Doherty DF, McAuley DF, Matthay MA, Kissenpfennig A, O'Kane CM, Krasnodembskaya AD. Mitochondrial Transfer via Tunneling Nanotubes is an Important Mechanism by Which Mesenchymal Stem Cells Enhance Macrophage Phagocytosis in the In Vitro and In Vivo Models of ARDS. *Stem Cells* 2016; 34: 2210-2223.

40. Puhm F, Afonyushkin T, Resch U, Obermayer G, Rohde M, Penz T, Schuster M, Wagner G, Rendeiro AF, Melki I, Kaun C, Wojta J, Bock C, Jilma B, Mackman N, Boilard E, Binder CJ. Mitochondria Are a Subset of Extracellular Vesicles Released by Activated Monocytes and Induce Type I IFN and TNF Responses in Endothelial Cells. *Circ Res* 2019; 125: 43-52.

41. Supinski GS, Schroder EA, Callahan LA. Mitochondria and Critical Illness. *Chest* 2020; 157: 310-322.

42. Harrois A, Huet O, Duranteau J. Alterations of mitochondrial function in sepsis and critical illness. *Curr Opin Anaesthesiol* 2009; 22: 143-149.

43. Hough RF, Islam MN, Gusarova GA, Jin G, Das S, Bhattacharya J. Endothelial mitochondria determine rapid barrier failure in chemical lung injury. *JCI Insight* 2019; 4.

44. Li X, Fang P, Mai J, Choi ET, Wang H, Yang XF. Targeting mitochondrial reactive oxygen species as novel therapy for inflammatory diseases and cancers. *J Hematol Oncol* 2013; 6: 19.

45. Piantadosi CA, Suliman HB. Mitochondrial Dysfunction in Lung Pathogenesis. *Annu Rev Physiol* 2017; 79: 495-515.

46. Kozlov AV, Lancaster JR, Jr., Meszaros AT, Weidinger A. Mitochondria-meditated pathways of organ failure upon inflammation. *Redox Biol* 2017; 13: 170-181.

47. Biswas S, Hwang JW, Kirkham PA, Rahman I. Pharmacological and dietary antioxidant therapies for chronic obstructive pulmonary disease. *Curr Med Chem* 2013; 20: 1496-1530.

48. Apostolova N, Victor VM. Molecular strategies for targeting antioxidants to mitochondria: therapeutic implications. *Antioxid Redox Signal* 2015; 22: 686-729.

49. Dushianthan A, Cusack R, Burgess VA, Grocott MP, Calder PC. Immunonutrition for acute respiratory distress syndrome (ARDS) in adults. *Cochrane Database Syst Rev* 2019; 1: CD012041.

50. Bos LDJ, Scicluna BP, Ong DSY, Cremer O, van der Poll T, Schultz MJ. Understanding Heterogeneity in Biologic Phenotypes of Acute Respiratory Distress Syndrome by Leukocyte Expression Profiles. *Am J Respir Crit Care Med* 2019; 200: 42-50.

51. Park J, Kim S, Lim H, Liu A, Hu S, Lee J, Zhuo H, Hao Q, Matthay MA, Lee JW. Therapeutic effects of human mesenchymal stem cell microvesicles in an ex vivo perfused human lung injured with severe E. coli pneumonia. *Thorax* 2019; 74: 43-50.

52. Hu S, Park J, Liu A, Lee J, Zhang X, Hao Q, Lee JW. Mesenchymal Stem Cell Microvesicles Restore Protein Permeability Across Primary Cultures of Injured Human Lung Microvascular Endothelial Cells. *Stem Cells Transl Med* 2018; 7: 615-624.

53. Varkouhi AK, Jerkic M, Ormesher L, Gagnon S, Goyal S, Rabani R, Masterson C, Spring C, Chen PZ, Gu FX, Dos Santos CC, Curley GF, Laffey JG. Extracellular Vesicles from Interferon-gamma-primed Human Umbilical Cord Mesenchymal Stromal Cells

Reduce Escherichia coli-induced Acute Lung Injury in Rats. *Anesthesiology* 2019; 130: 778-790.

54. Tang XD, Shi L, Monsel A, Li XY, Zhu HL, Zhu YG, Qu JM. Mesenchymal Stem Cell Microvesicles Attenuate Acute Lung Injury in Mice Partly Mediated by Ang-1 mRNA. *Stem Cells* 2017; 35: 1849-1859.

55. Monsel A, Zhu YG, Gennai S, Hao Q, Hu S, Rouby JJ, Rosenzwajg M, Matthay MA, Lee JW. Therapeutic Effects of Human Mesenchymal Stem Cell-derived Microvesicles in Severe Pneumonia in Mice. *Am J Respir Crit Care Med* 2015; 192: 324-336.

56. Hao Q, Gudapati V, Monsel A, Park JH, Hu S, Kato H, Lee JH, Zhou L, He H, Lee JW. Mesenchymal Stem Cell-Derived Extracellular Vesicles Decrease Lung Injury in Mice. *J Immunol* 2019; 203: 1961-1972.

Figure Legends

Figure 1. Characterization of MSC-derived extracellular vesicles (MSC-EVs). A, Characterization of MSC-EVs using nanoparticle tracking analysis (histogram generated from five independent measurements). **B**, Representative Transmission Electron Microscopy images showing: multivesicular bodies (upper left, scale bar 50 nm), exosomes (bottom left, scale bar 100 nm), mitochondria like structures (upper right, scale bar 1µm) and mitochondria like structures (bottom right, scale bar 200 nm). The images were taken using TEM microscope (JEOL, JEM 1400Plus, Japan). **C**, Immunoblot for protein expression levels of TOM20 in MSC-EVs and MSC-EVs-Rho lysates. All lanes were loaded with the same amount of total protein. **D**, Representative flow cytometry plots of MSC-EVs conjugated with 4µm beads demonstrating presence of EVs populations double positive for CD44 and MitoTracker Deep Red FM (19.1%) and EV populations double positive for CD63 and MitoTracker Deep Red FM (23.8%). **E**, Representative histogram of nanoparticle tracking analysis of EVs isolated from Rhodamine-6G pre-treated MSC (histogram generated from five independent measurements). **F**, Immunoblot for protein expression levels of TOM20 in Rho-EVs lysates. All lanes were loaded with the same amount of total protein as in **C**.

Figure 2. MSC-EVs improve barrier integrity of human primary lung epithelial and endothelial cells through transfer of functional mitochondria. A, Representative live images of MSC-EVs mitochondria internalisation in HSAECs and HPMECs cells [Scale bars 50 nm(left panel) and 10 nm (right panel)]. **B-C,** M1 coefficient co-localisation in HSAECs (**B**) and HPMECs, (**C**) The images were taken using a Nikon 6D Eclipse Ti-E inverted microscope with Okolab touch temperature unit and CO2 environmental chamber (Nikon Instruments, Japan) (40x dry super plan fluor ELWD objective with 0.6 NA). Data are mean ± s.d. of ten images frames**. D-E,** Levels of interleukin (IL)-8 secretion by HSAECs (**D**) and HPMECs (**E**). **F**, Representative real-time impedance analysis of HSAECs exposed to LPS

and treated with MSC-EVs or MSC-EVs-Rho. **G,** Cell impedance of HSAECs of XCelligence RTCA measurements. Data are mean ± s.d. (n = 3). **H**, Representative real-time impedance analysis of HPMECs exposed to LPS and treated with MSC-EVs or MSC-EVs-Rho. **I,** Cell impedance of HPMECs of XCelligence RTCA measurements. Data are mean ± s.d. (n = 3). ns, not significant, *P<0.05, **P<0.01, ***P<0.001, ****P<0.0001. Kruskal-Wallis test with post-hoc Dunn's test (**D,E**). One-way ANOVA analysis with post-hoc Bonferroni's test (**G,I**).

Figure 3. LPS induces mitochondrial dysfunction in human primary lung epithelial and endothelial cells which is alleviated by transfer of functional mitochondria in MSC-EVs. **A**, Representative live images of JC-1 dye fluorescence as an indicator of mitochondrial membrane potential in HSAECs and HPMECs after exposure to LPS and treatment with MSC-EVs or MSC-EVs-Rho for 24 hours. White arrows pointing at the areas of depolarized mitochondrial membranes (JC-1 monomers) and red arrows indicating polarized mitochondrial membranes (JC-1 aggregates). FCCP was used as a control for mitochondria depolarisation. The images were taken using a Nikon 6D Eclipse Ti-E inverted microscope (Scale bar,100 µm). **B,C**, Quantification of red/green fluorescence intensity ratio in HSAECs (**B**) and HPMECs (**C**). Data presented as mean ± SD of ten images. **D**, Representative live images of HSAECs and HPMECs of mitochondrial superoxide production detected with MitoSOX after exposure to LPS and treatment with MSC-EVs or MSC-EVs-Rho for 24 hrs or pre-treated with MitoTempo (Mt), 4 hrs prior stimulation. White arrows demonstrating mitochondrial ROS formation in HSAECs and HPMECs. The images were taken using a Nikon 6D Eclipse Ti-E inverted microscope (Scale bar,100 µm). **E-F,** Quantitative fluorescence intensity of MitoSOX in HSAECs (**E**) and HPMECs (**F**). Data presented as mean ± SD of ten images. **G,** Representative Seahorse Mito Stress assay showing oxygen consumption rate (OCR) in HSAECs. **H-J,** Calculated values for respiratory parameters: basal respiration (**H**), maximal respiration (**I**) and ATP production (**J**), (n=3). **K**, Representative Seahorse Mito Stress assay showing oxygen consumption rate (OCR) in HPMECs. **L-N** Calculated values for respiratory parameters: basal respiration (**L**), maximal respiration (**M**) and ATP production (**N**), (n = 3). Data presented as mean ± SD, ns, not significant, *P<0.05, **P<0.01, ***P<0.001, ****P<0.0001. Kruskal-Wallis test with post-hoc Dunn's test(**C,D,F,G**). One-way ANOVA analysis with post-hoc Bonferroni's test (**H,I,J,L,M,N**).

Figure 4. Inflammatory environment perturbs mitochondrial homeostasis in human primary lung epithelial and endothelial cells which is alleviated by MSC-EVs. A, Representative confocal microscopy of HSAECs and HPMECs showing the nucleus (DAPI), mitochondria (red) and LC3-II (green) in different experimental conditions. Arrows indicate co-localisation, indicating incorporation of mitochondria into autophagosome. The images were taken using Leica SP8 confocal microscope with a 40× oil-immersion objective (Scale bar = 50 µm). **B,C,** Mitophagy assessed by co-localisation of mitochondria specific red fluorescence with green autophagosome marker LC3-II in HSAECs (**B**) and HPMECs (**C**). Data are mean ± SD. of ten image frames. **D,** Representative confocal microscopy showing biogenesis of mitochondria in HSAECs and HPMECs cells. Arrow points at the cytoplasmic accumulation of BrdU-positive mtDNA. The images were taken using Leica SP8 confocal microscope with a 40× oil-immersion objective (Scale bar = 50 µm). **E,F,** Quantification of the ratio of BrdU-positive mtDNA per cytoplasm volume in HSAECs (**E**) and HPMECs (**F**) cells. Data are mean ± SD. of ten image frames. ns, not significant, *P<0.05, **P<0.01, ***P<0.001, ****P<0.0001. Kruskal-Wallis test with post-hoc Dunn's test.

Figure 5. MSC-EVs inhibit inflammatory response and restore mitochondrial function through mitochondrial transfer in human lung tissue in *ex vivo* cultured Human Precision Cut Lung Slices (PCLSs). A, Levels of interleukin(IL)-8 secretion in PCLSs supernatants at 24hrs after exposure to LPS (n=6-8, 3 donors). **B**, Levels of Tumor Necrosis Factor (TNF)-α secretion in PCLSs supernatants at 24hrs after exposure to LPS (n=6-8, 3 donors). **C**, Levels of Receptor for Advanced Glycation End Products (RAGE) secretion in PCLSs supernatants at 24hs after exposure to LPS (n=6-8, 3 donors). **D,** PCLSs viability measured by LDH release (n=8-10, 3 donors). **E,** Representative live images of JC-1 fluorescence in PCLSs as an indicator of mitochondrial membrane potential. FCCP was used as positive control for complete mitochondrial membrane depolarization. White arrows point at the areas with low mitochondrial membrane potential (accumulation of JC-1 monomers) and orange arrows point at the areas of normally polarised mitochondrial membranes (accumulation of JC-1 aggregates) in lung tissue. The images were taken using a Nikon 6D Eclipse Ti-E inverted microscope (Scale bar = 1mm). **F,** Quantification of red to green JC-1 fluorescence ratio in PCLSs was analyzed by ImageJ software. Data represented as mean ± s.d. of ten image frames. **G,** Representative images of mitochondrial superoxide production detected with MitoSOX in PCLSs. The images were taken using a Nikon 6D Eclipse Ti-E inverted microscope (Scale bar = 1mm). **H,** Quantitative fluorescence intensity was analyzed

by ImageJ software. Data represented as mean ± s.d. of ten image frames. **I,** Representative seahorse mito stress test assay showing oxygen consumption rate (OCR) in PCLSs. **J-L,** Calculated values were normalized to control PCLSs for respiratory parameters: basal respiration (**J**), maximal respiration (**K**) and ATP production (**L**). (n=3 independent experiments, 3 donors). Data represented as mean ± SD, ns, not significant, *P<0.05, **P<0.01, ***P<0.001, ****P<0.0001. Kruskal-Wallis test with post-hoc Dunn's test.

Figure 6. MSC-EVs modulate inflammatory response and partially restore epithelial and endothelial barrier properties via mitochondrial transfer in ARDS environment *in vitro*. A,B, Levels of IL-8 secretion by HSAECs (**A**) and HPMECs (**B**) at 24hrs in both types of ARDS plasma (n=3). **C,** Representative real-time impedance analysis of HSAECs exposed to hypo-inflammatory ARDS plasma. **D,** Cell impedance analysis of XCelligence RTCA measurements in HSAECs (n=3). **E,** Representative real-time impedance of HPMECs exposed to hypo-inflammatory ARDS plasma. **F,** Cell impedance analysis of XCelligence RTCA measurements in HPMECs (n=3). **G,** Representative real-time impedance of HSAECs exposed to hyper-inflammatory ARDS plasma. **H,** Cell impedance analysis of XCelligence RTCA measurements in HSAECs (n=3). **I,** Representative real-time impedance analysis of HPMECs exposed to hyper-inflammatory ARDS plasma samples. **J,** Cell impedance analysis of XCelligence RTCA measurements in HPMECs (n=3). **K,L,**. Calculated values for mitochondrial ATP production of HSAECs (**K**) and HPMECs (**L**) in both ARDS microenvironments (n=3). Data represented as mean ± SD, *P<0.05, **P<0.01, ***P<0.001, ****P<0.0001. Kruskal-Wallis test with post-hoc Dunn's test.

Figure 7. MSC-EVs downregulate levels of Ang-2 secretion by human primary lung epithelial and endothelial cells. A, Levels of Angiopoetin(Ang)-2 secretion in HPMECs supernatants at 24hrs after exposure to LPS (n=4) and treated with PBS, MSC-EVs, MSC-EVs-Rho or Mitotempo (Mt). **B,** Levels of Angiopoetin(Ang)-2 secretion in HSAECs supernatants at 24hrs after exposure to LPS (n=5) and treated with PBS, MSC-EVs, MSC-EVs-Rho or Mitotempo (Mt). **C,** Levels of of Angiopoetin(Ang)-2 secretion in HPMECs supernatants at 24hrs in both types of ARDS plasma (n=3) and treated with PBS, MSC-EVs, MSC-EVs-Rho or Mitotempo (Mt). **D,** Levels of of Angiopoetin(Ang)-2 secretion in HSAECs supernatants at 24hrs in both types of ARDS plasma (n=5) and treated with PBS, MSC-EVs, MSC-EVs-Rho or Mitotempo (Mt). Data represented as mean ± SD,*P<0.05, **P<0.01. Kruskal-Wallis test with post-hoc Dunn's test.

Figure 8. MSC-EVs reduce LPS-induced lung injury and restore mitochondrial respiration in the murine lung tissue *in vivo*. A, Total protein concentrations in the BALF samples (n=8-10 mice per group). **B-D**, Total cells counts (**B**), Absolute mononuclear cell counts (**C**) and Absolute neutrophil cell counts (**D**) in the BALF samples (n=6 mice per group). **E,** Representative images of BALF cytospin preparations demonstrating inflammatory cell recruitment to the airspaces were taken using the Leica Epifluorescence DM5500 microscope (original magnification, x20). **F,** BALF levels of tumor necrosis factor alpha (TNF-a). **G,** BALF levels of keratinocyte-derived chemokine (KC, murine analogue of IL-8) **H**, Schematic representation of generation of murine precision cut-lung slices (mPCLSs). **I**, Representative Seahorse Mito Stress test assay showing oxygen consumption rate (OCR) in mPCLSs. **J-L,** Calculated values for basal respiration (**J**), maximal respiration (**K**) and ATP production (**L**) of mPCLSs. Data represented as mean ±SD *P<0.05, **P<0.01, ***P<0.001, ****P<0.0001. Kruskal-Wallis test with post-hoc Dunn's test.

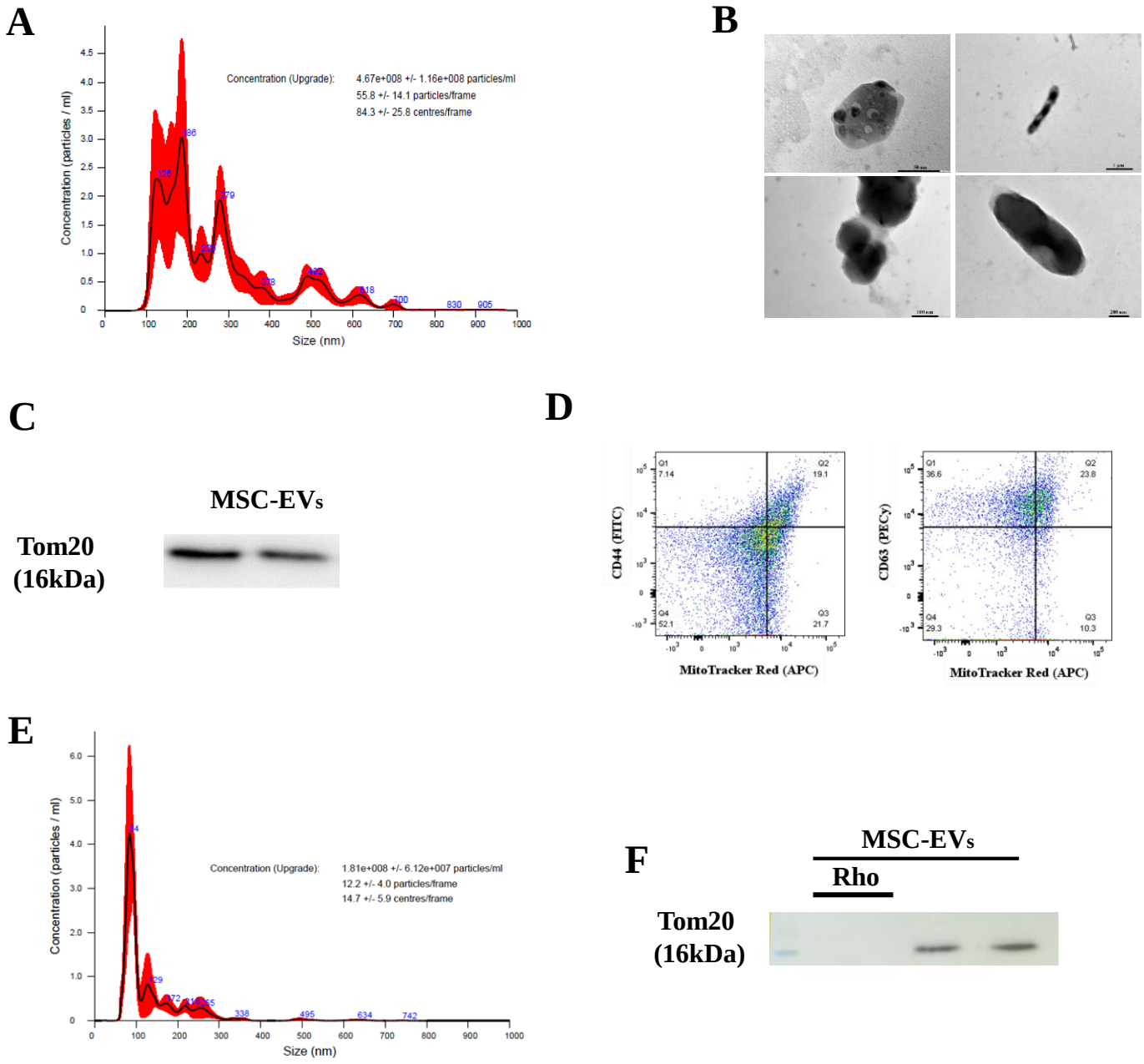

Figure 1.

Characterization of MSC-derived extracellular vesicles (MSC-EVs). A, Characterization of MSC-EVs using nanoparticle tracking analysis (histogram generated from five independent measurements). **B**, Representative Transmission Electron Microscopy images showing: multivesicular bodies (upper left, scale bar 50 nm), exosomes (bottom left, scale bar 100 nm), mitochondria like structures (upper right, scale bar 1µm) and mitochondria like structures (bottom right, scale bar 200 nm). The images were taken using TEM microscope (JEOL, JEM 1400Plus, Japan). **C**, Immunoblot for protein expression levels of TOM20 in MSC-EVs and MSC-EVs-Rho lysates. All lanes were loaded with the same amount of total protein. **D**, Representative flow cytometry plots of MSC-EVs conjugated with 4µm beads demonstrating presence of EVs populations double positive for CD44 and MitoTracker Deep Red FM (19.1%) and EV populations double positive for CD63 and MitoTracker Deep Red FM (23.8%). **E**, Representative histogram of nanoparticle tracking analysis of EVs isolated from Rhodamine-6G pre-treated MSC (histogram generated from five independent measurements). **F**, Immunoblot for protein expression levels of TOM20 in Rho-EVs lysates. All lanes were loaded with the same amount of total protein as in **C**.

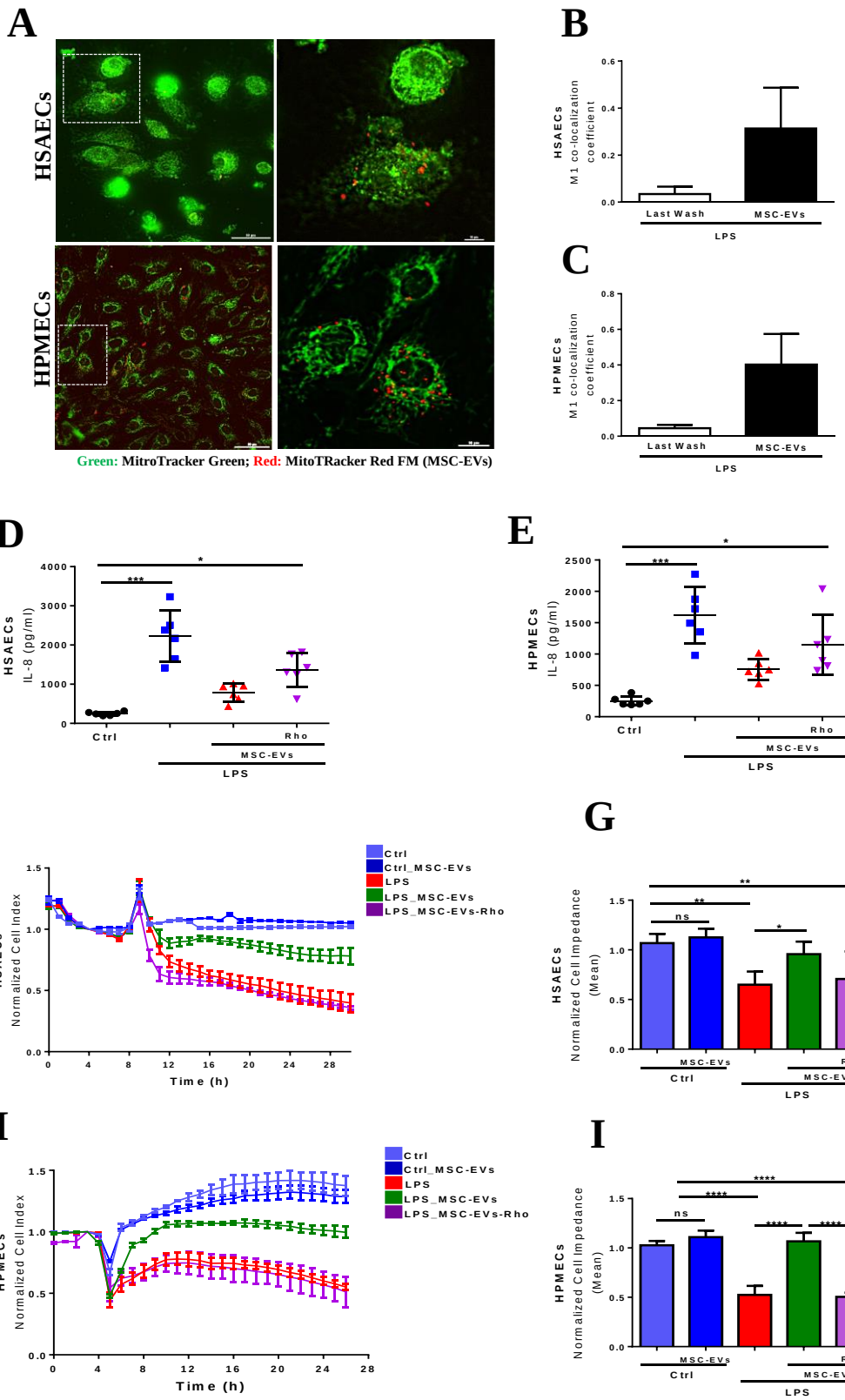

Figure 2. MSC-EVs improve barrier integrity of human primary lung epithelial and endothelial cells through transfer of functional mitochondria. **A**, Representative live images of MSC-EVs mitochondria internalisation in HSAECs and HPMECs cells [Scale bars 50 nm(left panel) and 10 nm (right panel)]. **B-C**, M1 coefficient co-localisation in HSAECs (**B**) and HPMECs, (**C**) The images were taken using a Nikon 6D Eclipse Ti-E inverted microscope with Okolab touch temperature unit and CO2 environmental chamber (Nikon Instruments, Japan) (40x dry super plan fluor ELWD objective with 0.6 NA). Data are mean ± s.d. of ten images frames. **D-E**, Levels of interleukin (IL)-8 secretion by HSAECs (**D**) and HPMECs (**E**). **F**, Representative real-time impedance analysis of HSAECs exposed to LPS and treated with MSC-EVs or MSC-EVs-Rho. **G**, Cell impedance of HSAECs of XCelligence RTCA measurements. Data are mean ± s.d. (n = 3). **H**, Representative real-time impedance analysis of HPMECs exposed to LPS and treated with MSC-EVs or MSC-EVs-Rho. **I**, Cell impedance of HPMECs of XCelligence RTCA measurements. Data are mean ± s.d. (n = 3). ns, not significant, *P<0.05, **P<0.01, ***P<0.001, ****P<0.0001. Kruskal-Wallis test with post-hoc Dunn's test (D,E). One-way ANOVA analysis with post-hoc Bonferroni's test (G,I).

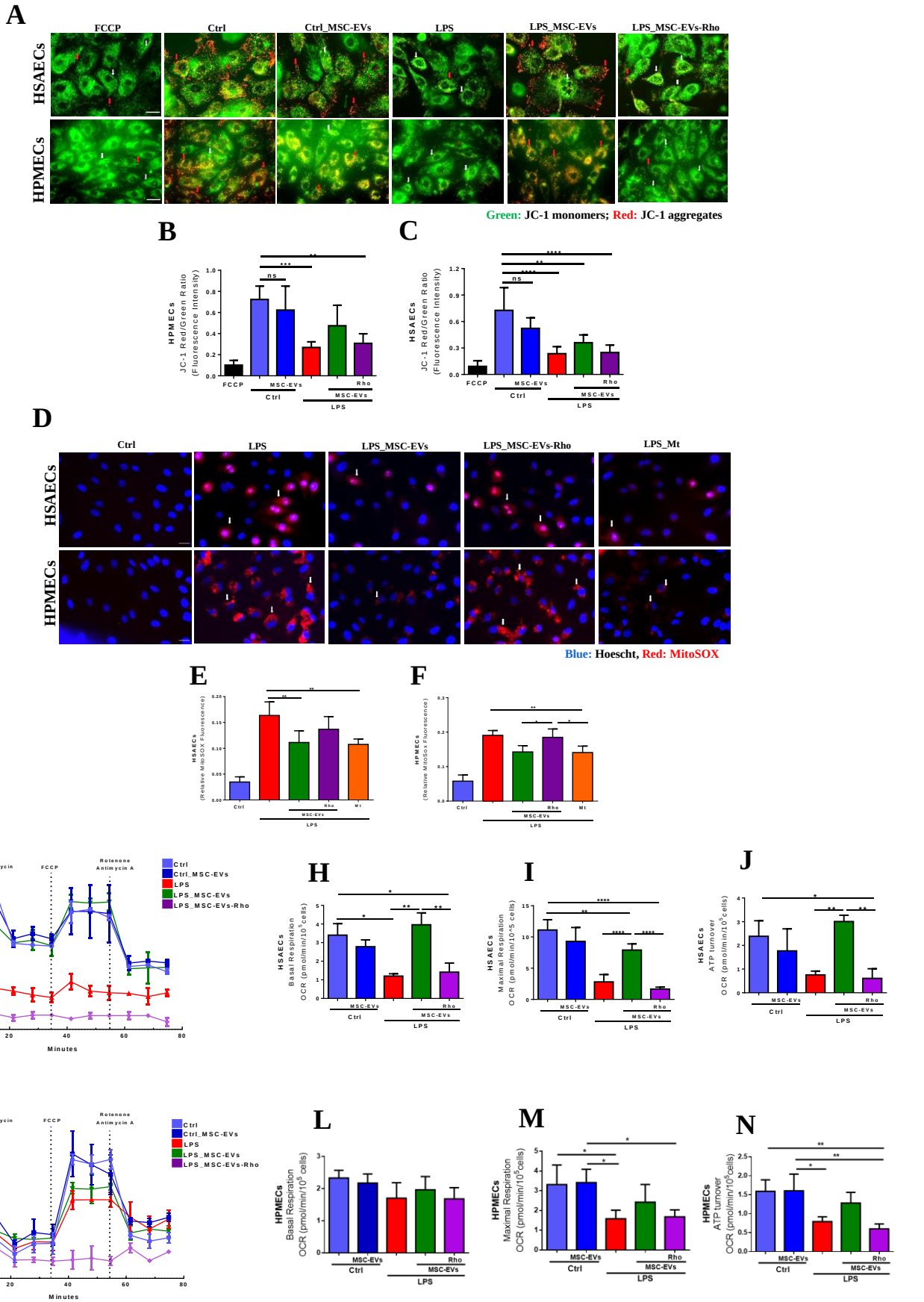

Figure 3. LPS induces mitochondrial dysfunction in human primary lung epithelial and endothelial cells which is alleviated by transfer of functional mitochondria in MSC-EVs. A, Representative live images of JC-1 dye fluorescence as an indicator of mitochondrial membrane potential in HSAECs and HPMECs after exposure to LPS and treatment with MSC-EVs or MSC-EVs-Rho for 24 hours. White arrows pointing at the areas of depolarized mitochondrial membranes (JC-1 monomers) and red arrows indicating polarized mitochondrial membranes (JC-1 aggregates). FCCP was used as a control for mitochondria depolarisation. The images were taken using a Nikon 6D Eclipse Ti-E inverted microscope (Scale bar,100 µm). **B,C**, Quantification of red/green fluorescence intensity ratio in HSAECs (**B**) and HPMECs (**C**). Data presented as mean ± SD of ten images. **D**, Representative live images of HSAECs and HPMECs of mitochondrial superoxide production detected with MitoSOX after exposure to LPS and treatment with MSC-EVs or MSC-EVs-Rho for 24 hrs or pre-treated with MitoTempo (Mt), 4 hrs prior stimulation. White arrows demonstrating mitochondrial ROS formation in HSAECs and HPMECs. The images were taken using a Nikon 6D Eclipse Ti-E inverted microscope (Scale bar,100 µm). **E-F,** Quantitative fluorescence intensity of MitoSOX in HSAECs (**E**) and HPMECs (**F**). Data presented as mean ± SD of ten images. **G,** Representative Seahorse Mito Stress assay showing oxygen consumption rate (OCR) in HSAECs. **H-J,** Calculated values for respiratory parameters: basal respiration (**H**), maximal respiration (**I**) and ATP production (**J**), (n=3). **K**, Representative Seahorse Mito Stress assay showing oxygen consumption rate (OCR) in HPMECs. **L-N** Calculated values for respiratory parameters: basal respiration (**L**), maximal respiration (**M**) and ATP production (**N**), (n = 3). Data presented as mean ± SD, ns, not significant, *P<0.05, **P<0.01, ***P<0.001, ****P<0.0001. Kruskal-Wallis test with post-hoc Dunn's test(**C,D,F,G**). One-way ANOVA analysis with post-hoc Bonferroni's test (**H,I,J, M,N**)

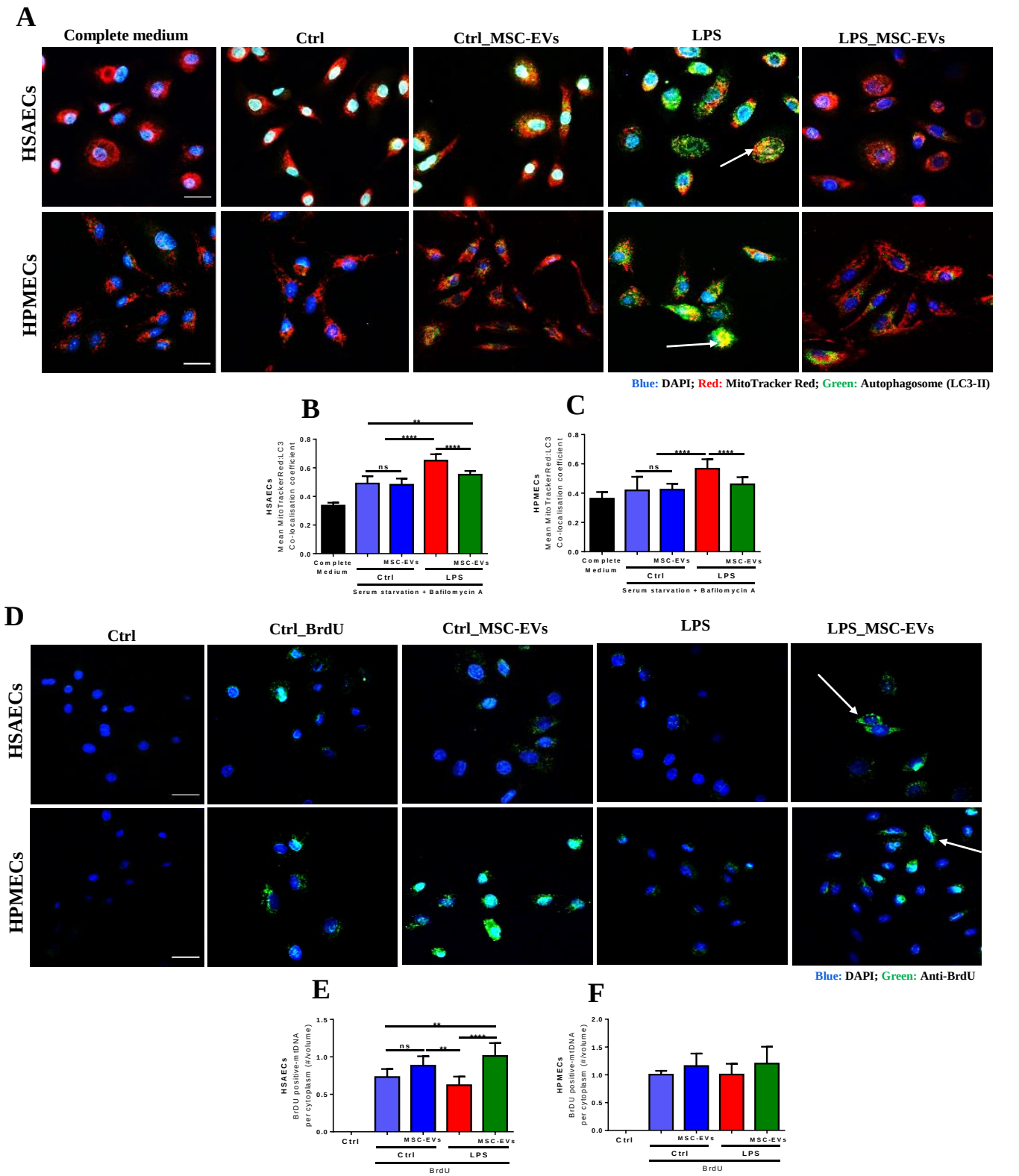

Figure 4. . Inflammatory environment perturbs mitochondrial homeostasis in human primary lung epithelial and endothelial cells which is alleviated by MSC-EVs. A, Representative confocal microscopy of HSAECs and HPMECs showing the nucleus (DAPI), mitochondria (red) and LC3-II (green) in different experimental conditions. Arrows indicate co-localisation, indicating incorporation of mitochondria into autophagosome. The images were taken using Leica SP8 confocal microscope with a 40× oil-immersion objective (Scale bar = 50 µm). **B,C,** Mitophagy assessed by co-localisation of mitochondria specific red fluorescence with green autophagosome marker LC3-II in HSAECs (**B**) and HPMECs (**C**). Data are mean ± SD. of ten image frames. **D,** Representative confocal microscopy showing biogenesis of mitochondria in HSAECs and HPMECs cells. Arrow points at the cytoplasmic accumulation of BrdU-positive mtDNA. The images were taken using Leica SP8 confocal microscope with a 40× oil-immersion objective (Scale bar = 50 µm). **E,F,** Quantification of the ratio of BrdU-positive mtDNA per cytoplasm volume in HSAECs (**E**) and HPMECs (**F**) cells. Data are mean ± SD. of ten image frames. ns, not significant, *P<0.05, **P<0.01, ***P<0.001, ****P<0.0001. Kruskal-Wallis test with post-hoc Dunn's test.

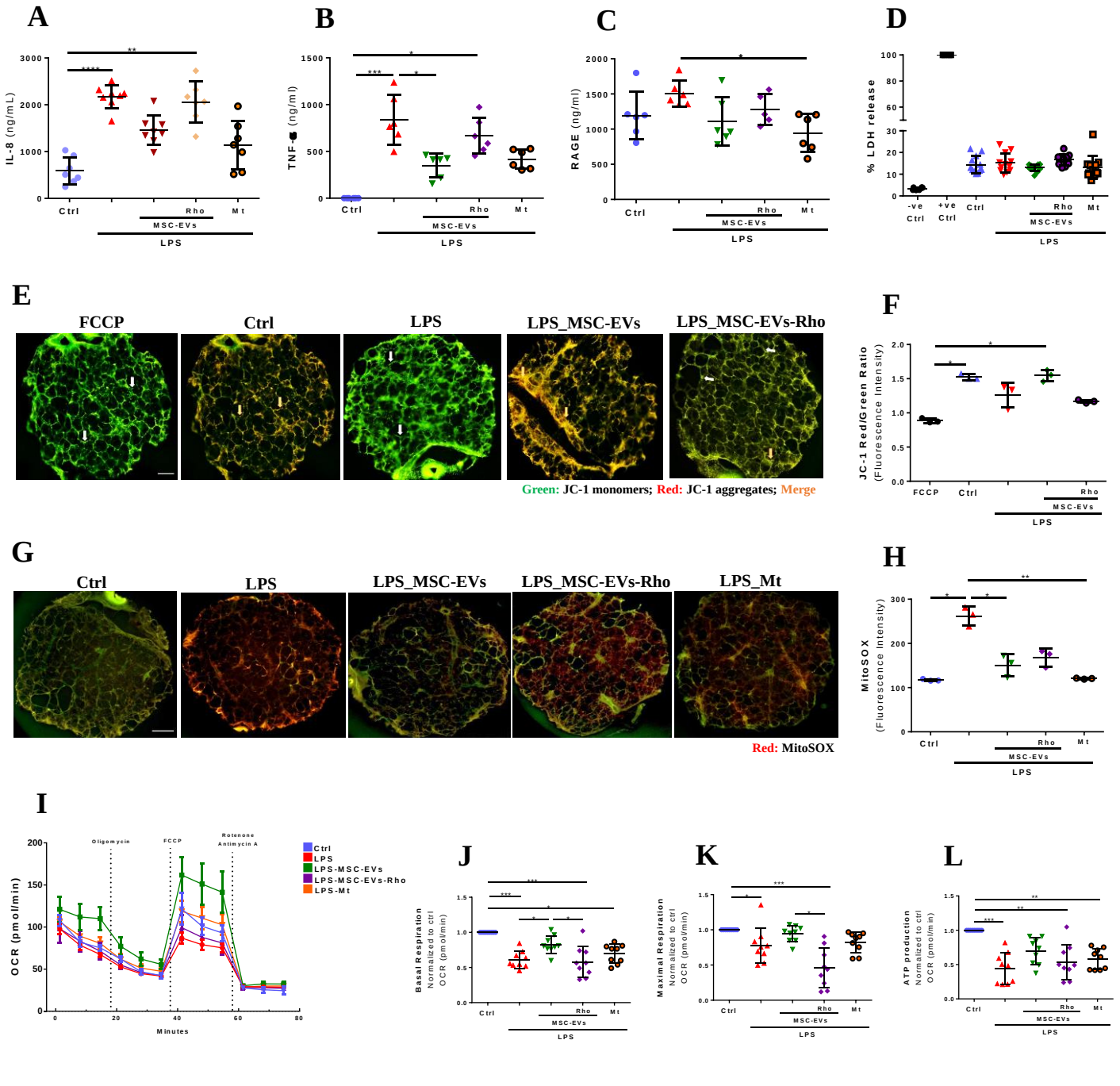

Figure 5. MSC-EVs inhibit inflammatory response and restore mitochondrial function through mitochondrial transfer in human lung tissue in *ex vivo* cultured Human Precision Cut Lung Slices (PCLSs). A, Levels of interleukin(IL)-8 secretion in PCLSs supernatants at 24hrs after exposure to LPS (n=6-8, 3 donors). **B**, Levels of Tumor Necrosis Factor (TNF)-α secretion in PCLSs supernatants at 24hrs after exposure to LPS (n=6-8, 3 donors). **C**, Levels of Receptor for Advanced Glycation End Products (RAGE) secretion in PCLSs supernatants at 24hs after exposure to LPS (n=6-8, 3 donors). **D,** PCLSs viability measured by LDH release (n=8-10, 3 donors). **E,** Representative live images of JC-1 fluorescence in PCLSs as an indicator of mitochondrial membrane potential. FCCP was used as positive control for complete mitochondrial membrane depolarization. White arrows point at the areas with low mitochondrial membrane potential (accumulation of JC-1 monomers) and orange arrows point at the areas of normally polarised mitochondrial membranes (accumulation of JC-1 aggregates) in lung tissue. The images were taken using a Nikon 6D Eclipse Ti-E inverted microscope (Scale bar = 1mm). **F,** Quantification of red to green JC-1 fluorescence ratio in PCLSs was analyzed by ImageJ software. Data represented as mean ± s.d. of ten image frames. **G,** Representative images of mitochondrial superoxide production detected with MitoSOX in PCLSs. The images were taken using a Nikon 6D Eclipse Ti-E inverted microscope (Scale bar = 1mm). **H,** Quantitative fluorescence intensity was analyzed by ImageJ software. Data represented as mean ± s.d. of ten image frames. **I,** Representative seahorse mito stress test assay showing oxygen consumption rate (OCR) in PCLSs. **J-L,** Calculated values were normalized to control PCLSs for respiratory parameters: basal respiration (**J**), maximal respiration (**K**) and ATP production (**L**). (n=3 independent experiments, 3 donors). Data represented as mean ± SD, ns, not significant, *P<0.05, **P<0.01, ***P<0.001, ****P<0.0001. Kruskal-Wallis test with post-hoc Dunn's test.

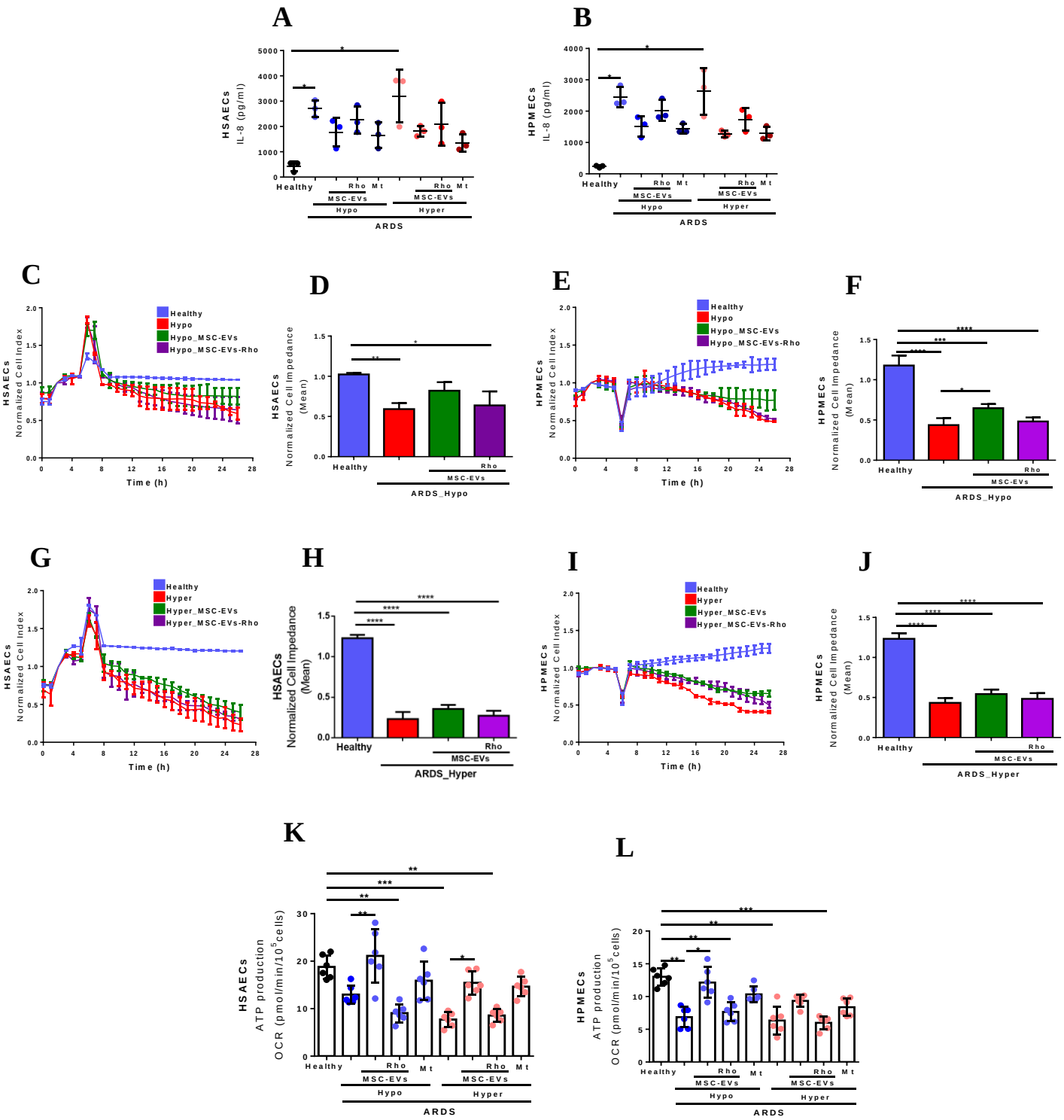

Figure 6. MSC-EVs modulate inflammatory response and partially restore epithelial and endothelial barrier properties via mitochondrial transfer in ARDS environment *in vitro*. A,B, Levels of IL-8 secretion by HSAECs (**A**) and HPMECs (**B**) at 24hrs in both types of ARDS plasma (n=3). **C,** Representative real-time impedance analysis of HSAECs exposed to hypo-inflammatory ARDS plasma. **D,** Cell impedance analysis of XCelligence RTCA measurements in HSAECs (n=3). **E,** Representative real-time impedance of HPMECs exposed to hypo-inflammatory ARDS plasma. **F,** Cell impedance analysis of XCelligence RTCA measurements in HPMECs (n=3). **G,** Representative real-time impedance of HSAECs exposed to hyper-inflammatory ARDS plasma. **H,** Cell impedance analysis of XCelligence RTCA measurements in HSAECs (n=3). **I,** Representative real-time impedance analysis of HPMECs exposed to hyper-inflammatory ARDS plasma samples. **J,** Cell impedance analysis of XCelligence RTCA measurements in HPMECs (n=3). **K,L,**. Calculated values for mitochondrial ATP production of HSAECs (**K**) and HPMECs (**L**) in both ARDS microenvironments (n=3). Data represented as mean ± SD, *P<0.05, **P<0.01, ***P<0.001, ****P<0.0001. Kruskal-Wallis test with post-hoc Dunn's test.

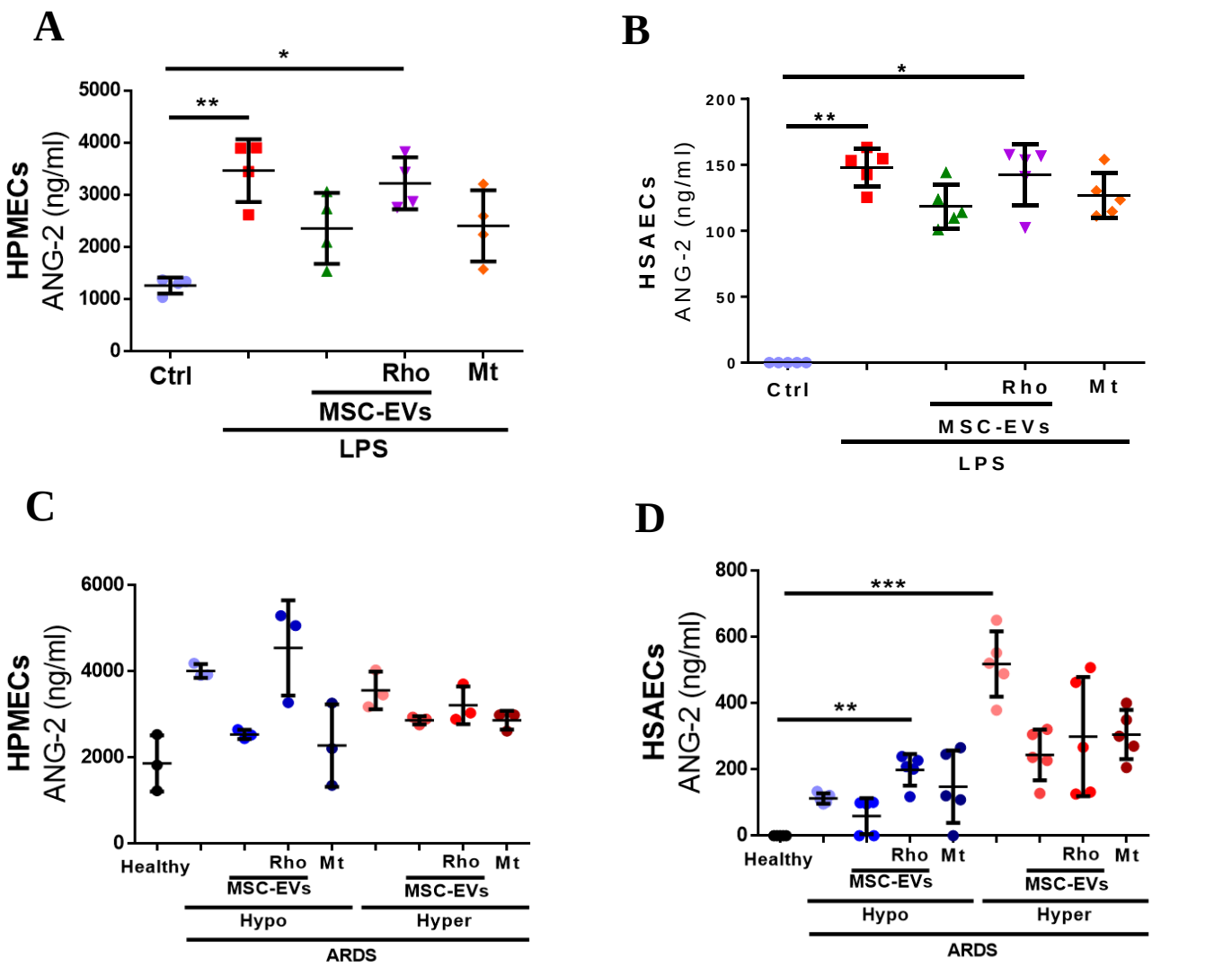

Figure 7. MSC-EVs downregulate levels of Ang-2 secretion by human primary lung epithelial and endothelial cells. A, Levels of Angiopoetin(Ang)-2 secretion in HPMECs supernatants at 24hrs after exposure to LPS (n=4) and treated with PBS, MSC-EVs, MSC-EVs-Rho or Mitotempo (Mt). **B,** Levels of Angiopoetin(Ang)-2 secretion in HSAECs supernatants at 24hrs after exposure to LPS (n=5) and treated with PBS, MSC-EVs, MSC-EVs-Rho or Mitotempo (Mt). **C,** Levels of of Angiopoetin(Ang)-2 secretion in HPMECs supernatants at 24hrs in both types of ARDS plasma (n=3) and treated with PBS, MSC-EVs, MSC-EVs-Rho or Mitotempo (Mt). **D,** Levels of of Angiopoetin(Ang)-2 secretion in HSAECs supernatants at 24hrs in both types of ARDS plasma (n=5) and treated with PBS, MSC-EVs, MSC-EVs-Rho or Mitotempo (Mt). Data represented as mean ± SD,*P<0.05, **P<0.01. Kruskal-Wallis test with post-hoc Dunn's test.

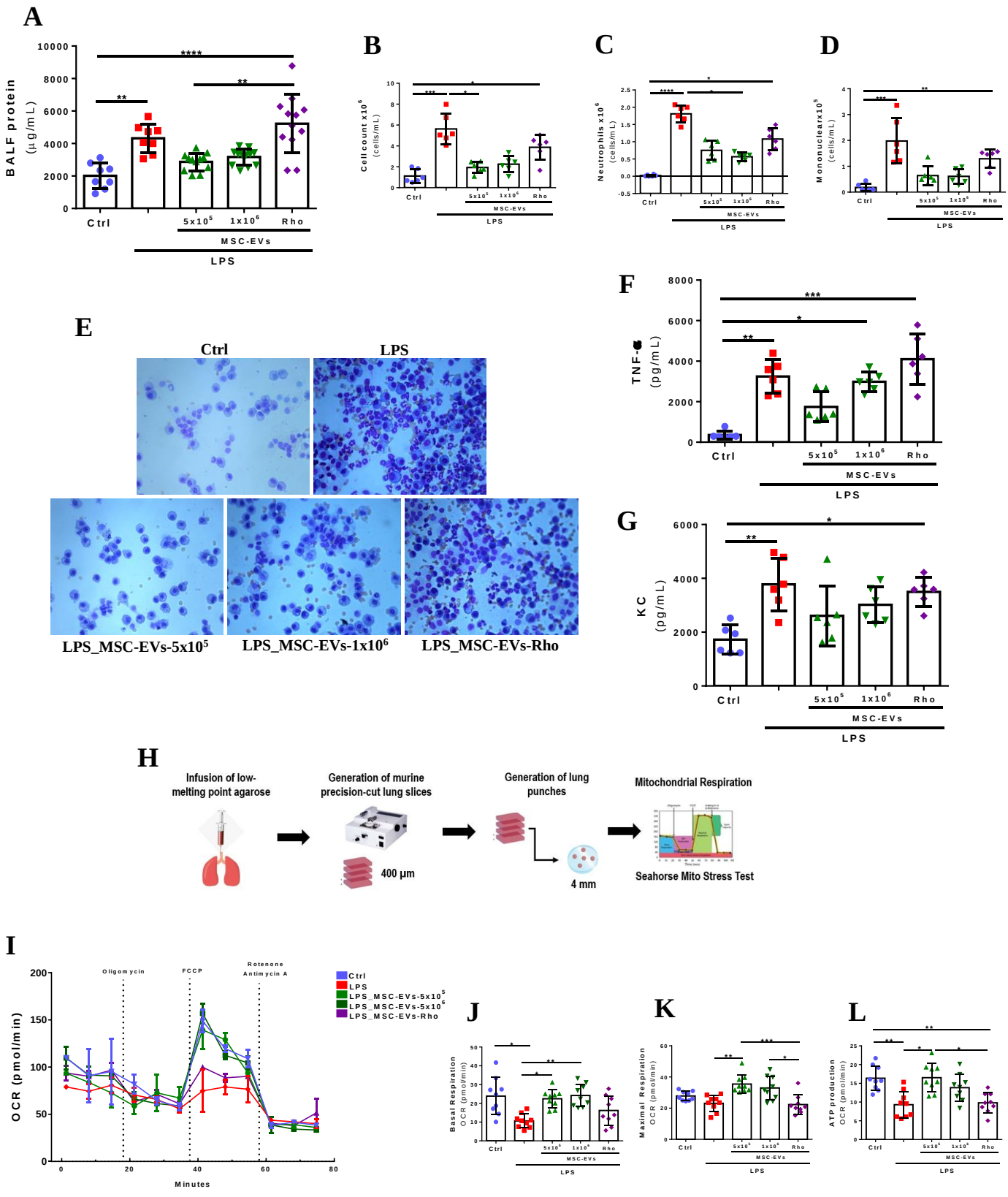

Figure 8. MSC-EVs reduce LPS-induced lung injury and restore mitochondrial respiration in the murine lung tissue *in vivo*. **A,** Total protein concentrations in the BALF samples (n=8-10 mice per group). **B-D**, Total cells counts (**B**), Absolute mononuclear cell counts (**C**) and Absolute neutrophil cell counts (**D**) in the BALF samples (n=6 mice per group). **E,** Representative images of BALF cytospin preparations demonstrating inflammatory cell recruitment to the airspaces were taken using the Leica Epifluorescence DM5500 microscope (original magnification, x20). **F,** BALF levels of tumor necrosis factor alpha (TNF-a). **G,** BALF levels of keratinocyte-derived chemokine (KC, murine analogue of IL-8) **H**, Schematic representation of generation of murine precision cut-lung slices (mPCLSs). **I**, Representative Seahorse Mito Stress test assay showing oxygen consumption rate (OCR) in mPCLSs. **J-L,** Calculated values for basal respiration (**J**), maximal respiration (**K**) and ATP production (**L**) of mPCLSs. Data represented as mean ±SD *P<0.05, **P<0.01, ***P<0.001, ****P<0.0001. Kruskal-Wallis test with post-hoc Dunn's test.

Supplementary Materials and Methods

Bone Marrow-derived Mesenchymal Stromal Cells (MSCs)

Human bone marrow-derived Mesenchymal Stromal Cells (MSCs) were obtained from American Type Culture Collection (ATCC® PCS-500-012). These cells had been extensively characterised in accordance with the standard laid out by the International Society for Cellular Therapy (ISCT) [1]. MSCs were cultivated in a T175 flask (ThermoFisher Scientific, UK) with 15 mL alpha-Minimum Essential Medium (α-MEM) supplemented with 16.5% heat-inactivated foetal calf serum (FCS), 1% L-glutamine amino acid (4mM) and 1% Penicillin/Streptomycin (50ug/mL) (all from Gibco, ThermoFisher Scientific, UK) and maintained at 37° C in a humidified tissue culture incubator at 5% CO_2 until used for experimentation. MSCs were fed every 2-3 days and sub-cultured into new flasks whenever 70-80% confluency was achieved. Upon reaching 80% confluence, media was aspirated from the flask of cells, washed with Phosphate Buffered Saline (DPBS) to remove any FCS-containing medium and MSCs were passaged with 0.05% trypsin-EDTA solution (Gibco, ThermoFisher Scientific, UK) for up to 5 minutes at 37° C until the cells had detached from the culture surface. Trypsin activity was neutralised by addition of α-MEM complete medium at a volume equal to that of the trypsin added to the flask, cells collected and centrifuged for 5 minutes at 1200 rpm. Following centrifugation, the supernatant was aspirated off and the cell pellet was resuspended in α-MEM complete medium. Cell viability, density and final concentration were then determined by Trypan Blue exclusion and by counting in a hemocytometer (Neubauer model). MSCs were used at passage 5. Multiple MSC donors were used for experiments through this study.

Human Primary Lung Small Airway Epithelial Cells (HSAECs) and Human Pulmonary Microvascular Endothelial Cells (HPMECs)

Human Primary Lung Small Airway Epithelial Cells (HSAECs) were obtained from PromoCell (PromoCell, Germany) in proliferating passage 2 and used to passage 8. These cells are isolated from the distal portion of the human respiratory tract in the 1 mm bronchiole area. They stain positive for cytokeratin. Cells were cultivated in small airway epithelial growth medium supplemented mix medium (PromoCell, Germany) (Table 1) and 1% Penicillin/Streptomycin (50ug/mL) (Gibco, ThermoFisher Scientific, UK). Human Pulmonary Microvascular Endothelial Cells (HPMECs) were obtained from PromoCell

(PromoCell, Germany) in proliferating passage 2 and used to passage 8. These cells were isolated from the lung blood and lymphatic capillaries microvascular endothelial cells. Cells were characterized by their expression of Cluster of Differentiation 31 (CD31) and Von Willebrand factor (VWF) and lack of expression of smooth muscle alpha-actin. HPMECs were cultivated in endothelial cell growth medium MV supplemented mix medium (PromoCell, Germany) (Table 1) and 1% Penicillin/Streptomycin (50ug/mL) (Gibco, ThermoFisher Scientific, UK).

HSAECs and HPMECs were cultivated in a T25 flask (ThermoFisher Scientific, UK) and maintained at 37° C in a humidified tissue culture incubator at 5% CO_2 until used for experimentation. Both cells type were passaged when they reached approximately 80% confluency. DetachKit (PromoCell, Germany) reagents were used at room temperature (RT). Media was aspirated from the culture flask, washed with 30mM HEPES Buffered Saline solution (HEPES-BSS; PromoCell, Germany), aspirated and the cells incubated with Trypsin-EDTA (0.04%/0.03%) solution for approximately 5 minutes at room temperature until the cells had detached from the culture surface. Trypsin was neutralised by adding a volume of Trypsin Neutralisation Solution (NTS; PromoCell, Germany) equal to the volume of trypsin. Detached cells were collected, centrifuged at 220g for 3 minutes. Following centrifugation, the supernatant was aspirated off and cell pellet resuspended in appropriated cell culture medium. Cell viability, density and final concentration were then determined by Trypan Blue exclusion and by counting in a hemocytometer (Neubauer model). Cells counted were seeded for experiments or culture flasks for expansion.

Table 1: Final concentrations of supplements after addition to basal medium

Small Airway Epithelial Cell Growth Medium	**Endothelial Cell Growth MV Medium**
0.004 mL/mL Bovine Pituitary Extract	0.05 mL/mL Fetal Calf Serum
10 ng/mL Epidermal Growth Factor (recombinant human)	0.004 mL/mL Endothelial Cell Growth Supplement
5 ug/mL Insulin (recombinant human)	10 ng/mL Epidermal Growth Factor (recombinant human)
0.5 ug/mL Hydrocortisone	90 ug/mL Heparin
0.5 ug/mL Epinephrine	1 ug/mL Hydrocortisone
6.7 ng/mL Triiodo-L-thyronine	
10 ug/mL Transferrin (recombinant human)	
0.1 ng/mL Retinoic Acid	
2.5 mg/mL Bovine Serum Albumin-Fatty Acid Free (BSA-FAF)	

Mesenchymal Stromal Cells-derived extracellular vesicles (MSC-EVs) isolation

The MSC-EVs ultracentrifugation was adapted from Zhu et al [2]. MSCs were grown to ~ 80% confluence in T175 flask under standard conditions. To prevent potential contamination with serum EVs, MSCs were cultured in 10 mL serum-free α-MEM supplemented medium for 48 hours to generate EVs. Conditioned medium (MSC-CM) was collected in 50 mL falcon tubes and centrifuged at 4° C for 2000 g for 45 minutes to remove cellular debris. The supernatant was transferred into polycarbonate ultracentrifuge tube (Beckman Coulter, US) ensuring that they were equally balanced. The tubes were attached to a 70 Ti rotor in Beckman Coulter ultracentrifuge (Optima Max- XP Ultracentrifuge, Beckman- Coulter, US) and centrifuged at 4° C for 100.000g for a further 3 hours to isolate MCS-EVs (acceleration =9 and deceleration = 5). The supernatant was gently aspirated, MSC-EVs gently washed with PBS and resuspended in PBS according to the final MSC cell count (EVs generated from 10^6 MSCs correspond to 10 µl of PBS).

MSC-EVs protein and RNA quantification

Quantification of MSC-EVs preparations was based on previously published work and findings in our group [3]. After MSC-EVs isolation, the concentration of RNA was assessed using the Nanodrop 2000 (ThermoFisher Scientific, UK) and protein assessed by BCA protein assay (Micro BCA protein assay kit, ThermoFisher Scientific, UK). 10 µl of MSC-EVs generated from $1x10^6$ MSC were used for *in vitro* experiments for each $1x10^4$ primary cells (HSAECs and HPMECs).

MSC-EVs measurements with Nanosight NS300

Size distribution and concentration of MSC-EVs were performed using Nanoparticle tracking analysis (NTA) device NanoSight NS300 (Malvern, UK). After MSC-EVs isolation from $1x10^6$ MSCs cell density, all samples were diluted in distilled water to a final volume of 1 mL. Settings were set according to the manufacturer's software manual (NanoSight NS300 User Manual). The detection threshold was determined to include as many particle as possible with the restrictions that 10-100 red crosses were counted while < 10% were not associated with distinct particles. Autofocus was adjusted so that indistinct particles were avoided. For each measurement, five 1-min videos were captured at 25° C. After capture, videos have been analysed by the in-build NanoSight Software NTA.

Visualisation of MSC-EVs morphology using transmission electron microscopy (TEM)

After MSC-EVs isolation, 500 µl of 4% paraformaldehyde (PFA) was added very slowly to the MSC-EVs pellet and incubated at RT for 30 minutes. After that, PFA was aspirated and washed three times with PBS for 10 minutes each. The MSC-EVs were resuspended in 30 µl of PBS and formvar/carbon-coated grids (Science Services, München) were loaded with 10 µl of sample. The grids and samples were incubated for 20 minutes at RT, dried on filter paper (Whatman, UK) and fixed with 2% glutaraldehyde for 10 minutes. Using non-magnetc tweezers, the grids were gently moved across five drops of distilled water for 1 minute each and dried between washes. After that, a drop of 1% tannic acid ACS reagent (Sigma Aldrich, UK) was added for 40 minutes at RT, washed two times in PBS for 1 minutes each, dried and then placed on a drop of TAAB EM heavy metal stain 336 (TAAB, Laboratory Equipment LTD, UK) for 30 minutes at RT. The grids were quickly submerged in 50% ethanol, washed in distilled water and dried. MSC-EVs were visualised on a TEM microscope (JEOL, JEM 1400Plus, Japan).

Characterization of MSC-EVs by Flow cytometry

For characterization by Flow cytometry, flow cytometry was realized with the addition of aldehyde/sulphate latex beads (ThermoFisher Scientific, UK) with 4um of diameter [4]. For mitochondrial identification, MitoTracker Deep Red FM (ThermoFisher Scientific, UK) was used for labelling mitochondria in MSCs respectively. MSC were grown in T175 to 80% confluence, washed with PBS to remove any residual FCS before staining and pre-stained with 200 nM of MitoTracker Deep Red FM in 10 mL serum-free α-MEM and incubated in 1x104 primary cells (HSAECs and HPMECs) 1x104 primary cells (HSAECs and HPMECs) the dark for 45 minutes. The dye-containing medium was aspirated, and the cells washed five times with PBS, 10 mL serum-free α-MEM supplemented medium was added for 48 hours to generate EVs as previously described. The latex beads were used to provide a reference point to compare with the EVs in FSC vs SSC plots. 100 µl of each fraction isolated were incubated with 0.25 µl of aldehyde/sulfate-latex beads ($ø = 4$ µm; 5.5×10^6 particles/ml) for 20 minutes at RT. Then 1 mL of PBS supplemented with 0.1% BSA (Roche) and 0.01% NaN_3 (G-Biosciences) was added and the sample incubated overnight on rotation. Bead-coupled EVs were centrifugated at 2000 g for 10 minutes, wash with 1 mL of BCB and centrifuged again. The pellet was resuspended with 100 µl of PBS and stained with anti-CD63 (Biolegend,) FITC-conjugated, anti-CD44 (eBioscience) PE-Cy7 conjugated primary

antibodies for 45 minutes at 4° C. Incubation of the beads-coupled EVs with respective isotype control Ab was used as negative controls. After incubation, MSC-EVs were washed twice and re-suspended in PBS. Gating of EV-decorated 4 µm in diameter beads was performed based on FCS/SSC parameters, so then unbound EVs or possible antibody aggregates were excluded from the analysis. Analysis was performed in FACS CantoII flow cytometer in FACSDiva software and data analysis was performed using FlowJo software (FlowJo, Ashland, OR).

Western blot analysis of MSC-EVs lysates

MSC-EVs obtained from healthy MSCs or MSCs with dysfunctional mitochondria (MSC-EVs-Rho) were lysed using Radioimmunoprecipitation assay (RIPA) buffer supplemented with cOmplete EDTA-free protease inhibitor (Sigma Aldrich) and phosphatase inhibitor PhosSTOP (Sigma Aldrich). The MSC-EVs were resuspended in 50 µl of RIPA buffer, incubated at 4° C for 30 minutes and placed in an ice-cold sonication for 1 minute. After that, gently mixed on ice for 2 minutes. Protein concentration was determined using BCA protein assay (Micro BCA protein assay kit, ThermoFisher Scientific, UK). 40 µg of total protein of each sample was separated on 10% SDS-PAGE under reducing conditions and transferred onto a PVDF membrane (GE Healthcare, Germany). The membranes were blocked with 5% milk and incubated with rabbit anti-human primary antibody anti-TOM20 (1:1000, Cell Signaling) overnight at 4° C. After washing, the blots were incubated with HRP-conjugated anti-rabbit IgG secondary antibody (1:1000, Cell Signaling) for 2h at RT. Protein expression was visualised using SuperSignal™ West Femto Maximum Sensitivity Substrate (ThermoFisher Scientific, UK) at G:Box Chemi imaging system (Syngene).

Generation of MSC-EVs dysfunctional mitochondria (MSC-EVs-Rho)

Loss-of-function experiments were performed to assess the importance of mitochondrial component of extracellular vesicles. To produce dysfunctional mitochondria, MSCs were treated with Rhodamine-6G (Sigma Aldrich) at a concentration of 1 µg/mL for 48 hours at 37° C. Once mitochondrial respiration would be blocked, MSCs had their medium supplemented to support glycolysis. Standard α-MEM was further supplemented with uridine (Sigma Aldrich) to produce a concentration of 50 ug/mL and sodium pyruvate to a concentration of 2.5 mM (Sigma Aldrich). After 48 hours, MSCs were washed five times with PBS and CM was generated for EVs isolation as previously described. MSC-EVs-Rho

were resuspended in PBS according to the final MSC cell count (EVs generated from 10^6 MSCs correspond to 10 µl of PBS). Size and concentration of MSC-EVs-Rho was quantified using NanoSight NS300 as previously described.

In vitro stimulation experiments

To generate an inflammatory microenvironment, *E. coli* lipopolysaccharide (LPS) 0111:B4 (Merck) was added to the HSAECs and HPMECs at working concentration of 1 µg/mL in 1% complete medium for 24 hours. In other experiments, plasma samples from ARDS patients recruited to the HARP-2 clinical trial were used for stimulation. These samples have been previously classified into 2 phenotypes based on concentration of inflammatory biomarkers [5] . Plasma samples from 20 patients (10 from each phenotype) were pooled to generate a stock and the pooled sample was then diluted in 1% complete medium to final concentration of 10% before stimulation. Plasma samples from healthy volunteers were used as control.

Studying mitochondrial transfer through MSC-EVs

For mitochondrial transfer study, MitoTracker fluorescent probes (ThermoFisher Scientific, UK) were used to label active mitochondria in MSCs. MSC were grown in T175 to 80% confluence, washed with PBS to remove any residual FCS before staining and pre-stained with 200 nM of MitoTracker Deep Red FM (ThermoFisher Scientific, UK) into 10 mL serum-free α-MEM and incubated in darkened conditions for 45 minutes. The dye-containing medium was aspirated, the cells were washed five times with PBS and 10 mL serum-free α-MEM supplemented medium was added for 48 hours to generate EVs as previously described. The last wash was stored and added to control wells to confirm that all residual staining was removed during wash steps. HSAECs and HPMECs at density of $1x10^4$ cells/well were plated in 96-well black plate with clear bottom (Nunc, ThermoFisher Scientific, UK) and incubated in normal cell cultured conditions to allow cell adhere to the plate. HPMECs or HSAECs were washed with HEPES-BSS and stained with 200 nM of MitoTracker Green (ThermoFisher Scientific, UK) in the dark for 45 minutes to stain endogenous mitochondria. After that, cells were washed and stimulated with *E.coli* LPS and treated with PBS, last wash collected from MSCs or MSC-EVs isolated from MSCs pre-stained with MitoTracker Deep Red FM for 24 hours to allow EVs uptake. Cells were washed three times and 100 µl of PBS was added. The images were taken using a Nikon 6D Eclipse Ti-E inverted microscope with Okolab touch temperature unit and CO_2 environmental

chamber (Nikon Instruments, Japan) (40x dry super plan fluor ELWD objective with 0.6 NA). 3D reconstruction of multiple z-stacks, deconvolution and video of microscopy images were done using Nikon 6D Eclipse software. The degree of colocalization of fluorescence signal originating from endogenous mitochondrial (MitoTracker Green) and MSC-EVs mitochondrial transfer (MitoTracker Deep Red FM) was quantified by calculating Manders' distinct colocalization coefficient M1 using Nikon 6D Eclipse software.

Epithelial and Endothelial permeability to FITC-Dextran

HSAECs and HPMECs were seeded at a density of $1x10^4$ cells/cm2 on transwell inserts with 0.4 µm pores suitable for a 24 well plate (Greiner). Cells were cultured at 37° C in a humidified tissue culture incubator at 5% CO_2 with medium changes every 2-3 days until confluent monolayer formation. Medium leak from the upper chamber into the lower chamber was analysed to confirm the confluence and ensure the formation of a good barrier. Following monolayer formation, cells were stimulated with *E.coli* LPS and treated with 10 µl of PBS, MSC-EVs or MSC-EVs-Rho for 24 hours. After that, medium was collected and stored for further analysis, 100 µl of 1% medium with 10 µl of 70 kDa FITC-Dextran (Sigma Aldrich) was added to the upper chamber and 500 µl of 1% medium to the lower chamber. A positive control in which FITC-Dextran was added to inserts on which no cells had been seeded was included. A blank in which PBS was added in place of FITC-Dextran to the upper chamber of inserts containing no cells was also included. Cells were kept in tissue culture incubator for 30 minutes, 100 µl samples from the lower chamber were collected and added to a 96-well black plate with clear bottom (Corning) in triplicate. Fluorescence intensity was read immediately using a FLUOstar Omega microplate reader at 485nm excitation and 520nm emission. Results are presented as % of positive control.

Cell impedance measurements in xCELLigence RTCA Single-Plate (SP) System

The xCELLigence RTCA SP system (Agilent) was used to measure, process and analyse the impedance (Cell index), which was detected by sensor electrodes in E-plate 16 (ACEA Biosciences). Before addition of cells, E-plate was coated with 2% gelatin (Sigma Aldrich), washed three times with PBS to remove the excess of gelatin and leave in the tissue culture hood to dry. The background was measured before seeding the cells in the E-plate, placed at 37° C in a humidified incubator at 5% CO_2 with 50 µl of 1% complete media. Then, 100 µl with $2x10^4$ HSAECs or HPMECs were seeded with 1% complete media and the plate was kept at RT for 1 hour to allow cells to adhere. After that, E-plate was set into RTCA SP

Station (ACEA Biosciences) in the CO_2 incubator and connected to the RTCA analyser. The baseline impedance was measured to ensure that all wells and connections were working within acceptable limits. As cells adhere to the E-plates, the Cell Index value increases from zero to a a maximum cell index of ~ 8 corresponding to very strongly adherent monolayer. Once cells measurements reach a plateau, the medium was changed and cells stimulated with *E.coli* LPS or plasma samples, treated with 20 µl of PBS, MSC-EVs or MSC-EVs-Rho for 24 hours. In separate experiments, before *E.coli* LPS or ARDS plasma samples stimulation, cells were pre-treated with 5 µM of MitoTempo (Mt), a mitochondria-targeted superoxide dismutase antioxidant, 4 hours prior stimulation. The cell index was recorded every 15 min for 24 hour. Every independent experiment was performed in triplicate. To demonstrate the effect of treatments, the cell index was normalized to equal value of cell index before adding the stimulations to making the values more comparable. The stimulated medium was collected and stored for further analysis.

Measurements of mitochondrial respiration

XFp96 analyzer from Seahorse Bioscience (Agilent) was used to determine cells' oxygen consumption rate (OCR) following manufacturer's instructions. HSAECs and HPMECs ($1x10^4$ cells/well) were plated 2 days before the assay into XFp cell culture mini-plates. Three replicate wells (technical triplicates) were used for each condition. During this incubation, a cartridge plate provided with the Cell Mito Stress Test Kit (Agilent Technologies) was soaked in XF calibrant solution and left to incubate at 37º C and 0% CO_2. 24 hours before measurements, cells were stimulated with *E.coli* LPS or plasma samples from ARDS endotypes and treated with 10 µl of PBS, MSC-EVs or MSC-EVs-Rho for 24 hours. In separated experiments, before *E.coli* LPS or ARDS plasma samples stimulation, cells were pre-treated with 5 µM of MitoTempo (Mt) 4 hours prior stimulation. After that, supernatant was collected and stored for further analysis and cells washed with HEPES-BSS. 180 µl of XF assay medium was added to each well at final concentration of 10 mM of Glucose, 1mM of Pyruvate and 2 mM of L-glutamine (all from Agilent), and placed in a humidified tissue culture incubator to incubate at 37º C and 0% CO_2 for 1 hour before experimentation. The mitochondrial stress test was performed using the following final concentrations of inhibitors: 1.0 µM oligomycin, 1.0 µM of carbonyl cyanide p-trifluoromethoxyphenylhydrazone (FCCP) and 0.5 µM of Rotenone/Antimycin-A (Rot/AA) (all from Agilent). After each inhibitor was added to the medium, three sequential measurements were taken. Each well was normalized to the percent of initial OCR. The

mitochondrial stress test parameters in mitochondrial stress test medium were calculated using the Wave software (Version 2.2) (Agilent Technologies) according to the manufacturer's instructions.

Determination of cell viability by Lactate Dehydrogenase (LDH) assay

LDH was quantified using Cytotoxicity Detection Kit (Roche) following manufactures instructions. Cell supernatants were centrifuged to remove cell debris at 5000 rpm for 10 minutes at 4º C. Supernatant was collected and 50 µl samples were added in triplicate into a 96-well plate (Nunc, ThermoFisher Scientific, UK). 50 µl of reaction mixture was added to the samples, mixed on a plate shaker for 1 minute and incubated for 30 minutes in the dark at RT. A positive control was included where cells were lysed with a final concentration of 2% Triton-X (Sigma Aldrich) 10 minutes before collection of supernatants. Optical densities were measured at 405nm using a FLUOstar Omega microplate reader. Data were analysed using MARS data analysis software. Results are presented as % relative to the positive control.

Enzyme-linked Immunosorbent Assay (ELISA)

Human TNF-α, IL-8, advanced glycosylation end-product specific receptor (RAGE) and human angiopoietin-2 (ANG-2) in cell and PCLS supernatants and murine TNF-α and keratinocyte chemoattractant (KC-murine IL-8 homolog) in broncho-alveolar lavage fluid were quantified using ELISA duoset kits (R&D System, Biotechne) according to manufacturer instructions. The ELISA plates were analyzed using Versamax spectrophotometer set to read at 450nm and 540nm wavelength. A subtraction of the wavelength absorbance readings at 540nm was taken from the readings at 450nm for correction. 4-parameter standard curves were produced using Softmax Pro v2.6 and concentrations of samples were extrapolated.

Investigation of mitochondrial biogenesis

5-bromo-2-deoxyuridine (BrdU, Sigma Aldrich) was used to assess the production of newly synthetised MtDNA within cells [6]. HSAECs and HPMECs were seeded in µ-slide 8-well chambers at density of $2x10^4$ cells per well and allowed to form a monolayer. A 10mM stock concentration of BrdU was diluted to a working concentration of 10 µM in 1% complete medium and added to the cells, *E. coli* LPS and treatment with 20 µl PBS, MSC-EVs or

MSC-EVs-Rho was added for 24 hours. After that, medium was collected and stored, cells washed with HEPES-BSS and fixed with 4% PFA for 15 minutes. After fixation, cells were washed and permeabilised with 0.1% Triton-X-100 (Sigma Aldrich) in 1x PBS for 15 minutes at RT. HSAECs and HPMECs DNA was denatured by adding 200 µl of 2N hydrochloric acid for 30 minutes at 37° C. To amplify the BrdU signal, a highly sensitive AlexaFluor 488 Tyramide SuperBoost Kit (ThermoFisher Scientific, UK) was used. Endogenous peroxidases were blocked with 100 µl 3% hydrogen peroxide solution for 30 minutes. After that, cells were washed and incubated with 100 µl 10% normal goat serum (NGS) supplied in the kit for 1 hour at RT to block non-specific antibody binding. A 1:50 dilution of purified monoclonal anti-BrdU antibody (0.5 mg/mL; Biolegend, UK) and the same concentration of IgG isotype control diluted in 1% NGS with 0.1% Tween 20 (Sigma Aldrich) were added to the wells and incubated overnight at 4° C. The wash step was repeated, cells incubated with 150 µl poly-HRP-conjugated secondary antibody supplied in the kit for 1 hour at RT. The wash step was repeated and 100 µl of tyramide solution was added to the cells and incubated for approximately 10 minutes at room temperature in the dark. The reaction was then terminated with a 1:11 dilution of stop reagent supplied in the kit and cells washed. The chamber was removed and coverslips were mounted on glass slides with Prolong Gold containing DAPI (ThermoFisher Scientific, UK). Fluorescence signals were viewed on the Leica SP8 confocal microscope with a 40× oil-immersion objective. Analysis of BrdU-labeled mtDNA was performed using Image J software. The cytosolic volume of each cell was measured by subtracting the volume of the nucleus from the total cell volume. All experiments were performed on cultured cells from at least three separate occasions with at least two replicates per condition.

Assessment of the mitophagy levels

The protocol for this experiment was adapted from Widdrington et al [7]. HSAECs and HPMECs were seeded in µ-slide 8-well chambers at density of $2x10^4$ cells per well and allowed to form a monolayer. Cells were stimulated with *E. coli* LPS and treated with 20 µl of PBS, MSC-EVs or MSC-EVs-Rho for 24 hours. Serum starved cells were used as a positive control for the induction of mitophagy and treatment with 5nM bafilomycin A1 (Sigma Aldrich) for 2h was used to prevent autophagosome turnover. 24 hours after cell stimulation, medium was collected and stored, cells were washed with HEPES-BSS and stained with 200 nM of MitoTracker Deep Red FM for 45 minutes at 37° C in the dark. After that, cells were washed and fixed with ice-cold 100% methanol at -20° C for 20 minutes.

After fixation, cells were incubated with 100 µl 5% FCS with 0.3% Triton X-100 in PBS for 1 hour at RT to block non-specific antibody binding. Cells were incubated with LC3-II primary antibody FITC conjugated (1:100; Cell Signaling) in 1% BSA with 0.3% Triton X-100 in 1x PBS overnight at 4° C in the dark. The wash step was repeated, cells counterstained with 300nM DAPI solution for 3 minutes at RT in the dark. The wash step was repeated, chamber was removed, and coverslips were mounted on glass slides with Prolong Gold Antifade Reagent (ThermoFisher Scientific, UK). Co-localisation of LC3A/B and endogenous mitochondria stained with MitoTracker Deep Red FM was determined using the Leica SP8 confocal microscope with a 40× oil-immersion objective. Co-localisation was assessed using the Mander's M1 co-localisation coefficient using Leica LAS X software.

Measurement of mitochondrial membrane potential

5,5',6,6'-tetrachloro-1,1',3,3'-tetraethylbenzimidazolylcarbocyanine iodide (JC-1) dye was used to assess mitochondrial membrane potential. This dye accumulates within mitochondria contingent on mitochondrial membrane potential. Red/green JC-1 fluorescence ratio is proportional to mitochondrial membrane potential. HSAECs and HPMECs were seeded at density of $1x10^4$ in 96-well black plate with clear bottom (Nunc) in triplicate and incubated in normal cell culture conditions to allow cell adhere to the plate. After stimulation, cells were washed and stained with JC-1 (Abcam) at a concentration of 20 µM diluted in 1x dilution buffer supplied in the kit for 15 minutes at 37° C in the dark. A control was included where 100 µM of FCCP was simultaneously added to the cells at the time of JC-1 staining to induce mitochondrial depolarisation. Following staining, wells were washed three times using 1x dilution buffer. 100 µl of PBS was added per well and live cells were immediately imaged at 20x magnification, using the EVOS FL Auto epifluorescent microscope. Red and green fluorescence intensity of each image was measured in ImageJ and the red/green ratio was calculated.

Detection of mitochondrial superoxide production in live cells

MitoSOX Red (ThermoFisher Scientific, UK) fluorescent dye allowing for a selective detection of superoxide in the mitochondria of live cells was used to detect mitochondrial superoxide production. HSAECs and HPMECs were seeded at density of $1x10^4$ in 96-well black plate with clear bottom (Nunc, ThermoFisher Scientific, UK) in triplicate and incubated in normal cell culture conditions to allow cell to adhere to the plate. Cells were stimulated with *E. coli* LPS or plasma samples from ARDS endotypes and treated with 10 µl of PBS,

MSC-EVs, MSC-EVs-Rho or pre-treated with 5 µM of MitoTempo (Mt), a mitochondria-targeted superoxide dismutase antioxidant, 4 hours prior stimulation. 24 hours after cell stimulation, supernatants were collected and stored, cells washed with HEPES-BSS and MitoSOX was added at 5 µM in the medium and incubated for 20 minutes at 37° C in the dark. Following staining, cells were washed three times, counterstained with 20 µM Hoechst (ThermoFisher Scientific, UK; for a final of 10 µM) and 100 µl of PBS was added per well. Live cells were immediately imaged at 20x magnification, using the EVOS FL Auto epifluorescent microscope. Red fluorescence intensity of each image was measured using ImageJ.

Generation of human Precision-Cut Lung Slices (PCLSs)

Lungs obtained from organ donors (where the organ has been unsuitable for transplantation, and next of kin has consented for use in research) were used for lung slices cultured *ex vivo*. Ethical approval has been given by National Review Ethics Service (NRES) in association with NHS Blood and Transplant for lungs obtained within the UK (REC 14/LO/0250). PCLSs were prepared from lung tissue donated by three donors. The protocol for PCLSs preparation was adapted from Franziska E. Uhl et al [8]. Lung segments were cannulated via a visible bronchus and filled with warm low gelling temperature agarose (2% by weight, Sigma, kept at 40°C) diluted in sterile cultivation medium (DMEM/Ham's F12; Gibco, supplemented with 100 U.mL-1 penicillin, 100 µg.mL-1 streptomycin, Sigma). Lungs segments were cooled on ice to allow gelling of the agarose. Cylindrical cores were separated using tissue coring tool, followed by cutting using a vibratome (Compresstome VF-300; Precisionary Instruments) to create 400 µm-thick slices. Incubation medium was changed every 30 min for 2 h after slicing, in order to remove residual agarose and cell debris from the tissue. The PCLSs were cultured in medium supplemented with 0.1% fetal calf serum (FCS) (Gibco) in 96 wells plates at 37° C in humidified incubator containing 5% CO_2 under submerged conditions with daily changes of medium. PCLSs were punched to a diameter of 4 mm using a biopsy punch, ensuring exclusion of major airways. Punches were taken from similar peripheral areas of the lung to minimise sample variation and standardise for tissue volume in further analysis.

***In vitro* stimulation of human PCLSs**

To generate an inflammatory microenvironment, *E. coli* LPS 0111:B4 (Merck) was added to the PCLSs at working concentration of 1 µg/mL in 1% complete medium for 24 hours.

PCLSs were treated with 10 µl of PBS, MSC-EVs, MSC-EVs-Rho (isolated from 10^6 MSCs) or pre-treated with 5 µM of MitoTempo (Mt), a mitochondria-targeted superoxide dismutase antioxidant, 4 hours prior stimulation. 24 hours after stimulation measurements was performed, supernatants were collected and stored for further analysed.

Viability of human PCLSs

Viability of tissue slices or 4 mm biopsy punches was checked by Lactate Dehydrogenase (LDH) assay using Cytotoxicity Detection Kit (Roche) as previously described. Results are presented as % relative to the positive control.

Measurement of mitochondrial respiration in human PCLSs

For measurement of mitochondrial respiration, 4 mm biopsy punches were cultured in the XF 96-well tissue culture plates. The Seahorse XF Cell Mito Stress Test Kit (Agilent Technologies) was used as previously described. The mitochondrial stress test was performed using the following final concentrations of inhibitors: 1.0 µM oligomycin, 1.0 µM of carbonyl cyanide p-trifluoromethoxyphenylhydrazone (FCCP) and 0.5 µM of Rotenone/Antimycin-A (Rot/AA) (all from Agilent). Oxygen consumption rate (OCR) readouts produced by the assay were analysed using the Wave software (Version 2.2) (Agilent Technologies).

Detection of mitochondrial membrane potential and mitochondrial superoxide production in human PCLSs

4 mm biopsy punches were used for measurements of mitochondrial membrane potential using JC-1staining and mitochondrial superoxide production using MitoSOX Red staining as described above. Images were taken using a Nikon 6D Eclipse Ti-E inverted microscope with and Okolab touch temperature unit and CO_2 environmental chamber (Nikon Instruments, Japan) (20x dry objective). The analysis was performed using ImageJ software.

Studying mitochondrial transfer through MSC-EVs in PCLSs

For mitochondrial transfer study, MitoTracker fluorescent probes (ThermoFisher Scientific, UK) were used to label active mitochondria in MSCs as previous described. PCLSs stimulated with E.coli LPS and treated with last wash collected from MSCs (PBS), MSC-EVs isolated from MSCs pre-stained with MitoTracker Deep Red FM or MSC-EVs-Rho for 24 hours to allow EVs uptake. PCLSs were washed three times with PBS, removed, and

coverslips were mounted on glass slides with Prolong Gold Antifade Reagent (ThermoFisher Scientific, UK). The images were taken using a Leica SP8-Upgright Confocal microscopy (original magnification x20 HC PL FLUOTAR, scale bar 50µm).

***In vivo* studies**

C57BL/6 mice (4 to 6 weeks old, Harland Institute, UK) were used. Animals were maintained in the Biological Service Unit (BSU) at Queen's University Belfast. Animals were housed in standard laboratory cages, with access to food and water *ad libitum*. Experiments were sanctioned and approved by the UK Home Office and Queen's University Belfast Ethical Review Committee.

Animal preparation and experimental protocol

Mice were anaesthetized with were anesthetized with 100 µL of xylazine/ketamine (0.25 $mg.kg^{-1}$ and 0.025 $mg.kg^{-1}$, respectively) intraperitoneally. Lung injury was induced by administering *E. coli* LPS O111:B4 (Merck) intratracheally (2mg/kg body weight) diluted in PBS at a volume of 50 µl. In control mice, sterile PBS was administered intratracheally (50 µl) instead. Four hours later, mice were then treated with vehicle control (PBS), MSC-EVs (isolated from $5x10^5$ or $1x10^6$ MSC cells, 50 µl diluted in PBS) or MSC-EVs-Rho ($1x10^6$, 50 µl diluted in PBS). Mice were observed until recovery and returned to holding. 24 hours after LPS instillation, mice were culled and BALF was collected for cell counts, protein quantification and cytokine analysis.

Bronchoalveolar lavage fluid

Mice were culled with intraperitoneal injection of xylazine/ketamine. Thereafter, the trachea was cannulated by 21-gauge needle and 1mL of PBS was instilled into the lungs. The PBS was gently flushed in and lifted out 3-5 times to ensure thorough sampling of the bronchoalveolar compartment was collected. BALF samples were centrifuged at 5000 g for 5 mins to remove the cells from suspension. Supernatants were collected and stored for future processing.

Bronchoalveolar Lavage Fluid (BALF) Cellularity and Total Protein Content

The cell pellet was resuspended in 300 µl of PBS and first diluted 2-fold. 20 µl of the diluted sample was mixed with 20 µl of trypan blue and then 10 µl was added to Neubauer chamber and total leukocyte counting was performed under light microscopy. BALF sample and

dilutions were accounted for the final counts expressed as cells/mL. After taking the aliquot for total cell counts, the cell pellet was centrifuged at 10,000 rpm for 5 mins using the StatSpin Cytofuge®2 (Beckman Coulter, VWR) onto microscope slides. Slides were given 2 hours to dry and then stained using the Speedy Diff kit (Clin-tech). Differential cell count was performed in cytospin smears using the Leica Epifluorescence DM5500 microscope at 20x magnification. Enough images were taken of each slide to count a total of 400 cells. Cells were counted using ImageJ software and the percentage of neutrophils was determined. The total protein content in the BALF supernatant was quantified by BCA protein assay (Micro BCA protein assay kit, ThermoFisher Scientific, UK).

Generation of murine PCLSC (mPCLs)

24 hours after LPS instillation, mice were culled with a mixture of xylazine /ketamine. The trachea was sectioned, cannulated with severed 18-gauge needle, the anterior chest wall was surgically removed, and the lungs exposed. Using a syringe, lungs were filled *in situ* with warm, low gelling temperature agarose (3% by weight, Sigma, kept at 40C) diluted in sterile cultivation medium (DMEM/Ham's F12; Gibco, supplemented with 100 U.mL-1 penicillin, 100 µg.mL-1 streptomycin, Sigma). The trachea was ligated with thread to retain the agarose inside the lung. The lung was excised, transferred into a 50 mL conical tube with cultivation medium and cooled on ice for 15 minutes to allow gelling of the agarose. The lobes were separated and cut with a vibratome to a thickness of 400 µM. A total of 12 to 15 slices were made per lung. After slicing, biopsies punches using a 4mm disposable biopsy punch were performed. The mPCLs were cultured in medium supplemented with 0.1% fetal calf serum (FCS) (Gibco) in 96 wells plates. Incubation medium was changed every 30 min for 2 h after slicing, to remove agarose residues and cell debris from the tissue.

Assessing mitochondrial respiration on mPCLSs

To evaluate mitochondrial respiration, the Seahorse XF Cell Mito Stress Test Kit (Agilent Technologies) was used as previously described. mPCLs punches were transferred into XF 96-well tissue culture plates. mPCLSs were washed with XF basal medium and 180 µl of XF basal medium was added to each well. Oligomycin, carbonyl cyanide-4 (trifluoromethoxy) phenylhydrazone (FCCP) and rotenone/antimycin-A inhibitors were prepared as per the manufacturer's instructions. Oxygen consumption rate (OCR) readouts produced by the assay were analysed using the Wave software (Version 2.2) (Agilent Technologies).

Statistical Analysis

Analysis was performed using GraphPad Prism 6 software (GraphPad Software, La Jolla, CA). Experiments were performed at least in triplicate, the average of three technical replicates was taken as a single data point for each donor, and the points were pooled together for statistical analysis. The Kolmogorov-Smirnov test with Lilliefors' correction was used to evaluate the homogeneity of variances. For parametric data, one-way analysis followed by post-hoc analysis using Bonferronis' was selected. For nonparametric data, the Kruskal-Wallis test followed by post-hoc using Dunns' comparisons was used. The statistical significance level was set as $p < 0.05$.

References

1. Dominici, M., et al., *Minimal criteria for defining multipotent mesenchymal stromal cells. The International Society for Cellular Therapy position statement.* Cytotherapy, 2006. **8**(4): p. 315-7.
2. Zhu, Y.G., et al., *Human mesenchymal stem cell microvesicles for treatment of Escherichia coli endotoxin-induced acute lung injury in mice.* Stem Cells, 2014. **32**(1): p. 116-25.
3. Morrison, T.J., et al., *Mesenchymal Stromal Cells Modulate Macrophages in Clinically Relevant Lung Injury Models by Extracellular Vesicle Mitochondrial Transfer.* Am J Respir Crit Care Med, 2017. **196**(10): p. 1275-1286.
4. Suarez, H., et al., *A bead-assisted flow cytometry method for the semi-quantitative analysis of Extracellular Vesicles.* Sci Rep, 2017. **7**(1): p. 11271.
5. Calfee, C.S., et al., *Acute respiratory distress syndrome subphenotypes and differential response to simvastatin: secondary analysis of a randomised controlled trial.* Lancet Respir Med, 2018. **6**(9): p. 691-698.
6. Lentz, S.I., et al., *Mitochondrial DNA (mtDNA) biogenesis: visualization and duel incorporation of BrdU and EdU into newly synthesized mtDNA in vitro.* J Histochem Cytochem, 2010. **58**(2): p. 207-18.
7. Widdrington, J.D., et al., *Exposure of Monocytic Cells to Lipopolysaccharide Induces Coordinated Endotoxin Tolerance, Mitochondrial Biogenesis, Mitophagy, and Antioxidant Defenses.* Front Immunol, 2018. **9**: p. 2217.
8. Uhl, F.E., et al., *Preclinical validation and imaging of Wnt-induced repair in human 3D lung tissue cultures.* Eur Respir J, 2015. **46**(4): p. 1150-66.

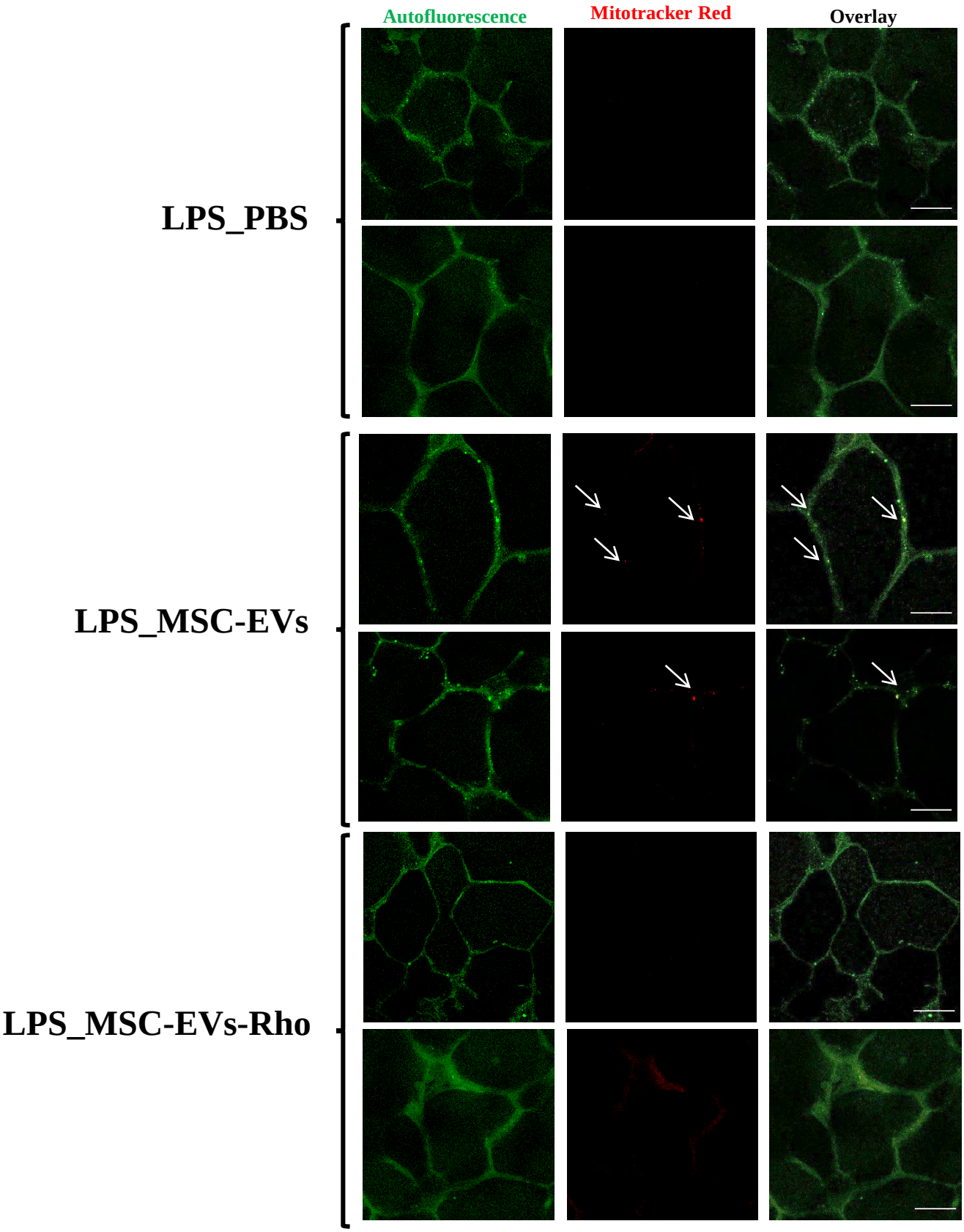

Supplementary Figure 1. Mitochondrial transfer through MSC-EVs to Human Precision Cut Lung Slices (PCLSs). Representative confocal images of MSC-EVs mitochondria transfer in PCLSs. PCLSs were stimulated with LPS and treated with PBS, MSCs pre-stained with MitoTracker Deep Red FM or MSC-EVs-Rho for 24 hours to allow EVs uptake. The images were taken using the Leica SP8-Upgright Confocal microscopy (scale bars 50 µm).